Journal of Industrial Information Integration 50 (2026) 101075

Contents lists available at ScienceDirect

Journal of Industrial Information Integration

journal homepage: www.elsevier.com/locate/jii

Full length article

Ensemble-based ship weather multi-objective route optimization

Kumars Mahmoodi [a,*], Jari Böling [b,a], Roberto Vettor [c]

[a] Faculty of Natural Sciences and Engineering, Åbo Akademi University, Turku, Finland
[b] Automation, Mechanical and Materials Engineering, University of Turku, Finland
[c] Napa Ltd., Tammasaarenkatu 3, 00180 Helsinki, Finland

ARTICLE INFO

Keywords:
Weather routing
Route optimization
Grey wolf optimizer
Weather uncertainty
Cruise ship

ABSTRACT

Many traditional and state-of-the-art ship routing methods rely on single-objective formulations, deterministic weather inputs, or fixed operational assumptions, which may lead to suboptimal or impractical routing decisions under realistic and uncertain marine environments. This study presents an ensemble-based multi-objective optimization framework for ship route planning under uncertain weather conditions. The framework integrates a neural network model, trained on real onboard ship performance data and tuned using Bayesian hyperparameter optimization, to predict fuel consumption based on ship speed and marine weather parameters. An ensemble of weather forecasts is assigned to route waypoints using a bootstrapping method, enabling the evaluation of multiple cost functions reflecting trade-offs between voyage time, fuel consumption, and safety. Four optimization objective strategies — ensemble mean, worst-case, risk-aware, and Conditional Value-at-Risk (CVaR) — are implemented within a Grey Wolf Optimizer (GWO) to derive optimal routes across various voyages. The results demonstrate notable variations in route performance based on the selected strategy. For example, the CVaR approach achieves a balance between robustness and efficiency, with voyage fuel consumption for the longest journey (Voyage 3) reaching 490,475 kg, while the worst-case strategy prioritizes risk-averse paths, resulting in the highest fuel usage at 505,308 kg. Conversely, the ensemble mean strategy offers the lowest average fuel consumption (474,078 kg) but may expose the voyage to higher uncertainty. Furthermore, the proposed GWO demonstrates high precision in schedule adherence, maintaining arrival time deviations within a 30-minute margin across all optimized voyages, thereby justifying its effectiveness in handling complex multi-objective constraints. The developed framework is applicable to real-time voyage optimization and can support ship operators in achieving fuel efficiency and safety under varying ocean conditions.

1. Introduction

The efficient and safe navigation of ships is critical for the global maritime industry. Optimization of ship routes has long been a key focus area, intending to reduce fuel consumption, minimize transit times, and ensuring safety under varying marine conditions. Ship fuel consumption is a vital factor influencing operational costs and environmental impact. An accurate estimation of ship fuel consumption is essential for optimizing performance, minimizing fuel expenses, and reducing greenhouse gas emissions [1]. Various factors contribute to ship weather routing and fuel consumption uncertainties, including dynamic environmental conditions (e.g., wind, waves, and currents), vessel speed, hull fouling, and operational efficiency [2]. These uncertainties make it challenging to ship routing and estimate fuel consumption with high precision, necessitating the consideration of uncertainty quantification techniques. Deterministic models often overlook the inherent variability in the inputs. Probabilistic approaches allow for the modeling of input uncertainties and provide a more comprehensive understanding of how these uncertainties affect the results [3].

Some key sources of uncertainties are provided in Fig. 1. Environmental uncertainties arise from different sources. Wind intensity and direction variations affect a ship's resistance and propulsion needs [4]. Wave height, period, and direction impact vessel motion and fuel consumption [5]. Changes in ocean currents can help or resist a vessel's motion, leading to uncertainty in fuel use. Shallow waters or strong tidal currents can influence resistance. Operational uncertainties are another source of uncertainties. Some of these factors are speed fluctuations due to operational constraints or weather-routing decisions, changes in the ship's weight distribution and total load which affect its resistance and fuel consumption, and differences in operating procedures and crew behaviors that can lead to variations in fuel efficiency [6]. Technical uncertainties such as ship hull condition, propulsion system efficiency, and fuel quality are other reasons for

* Corresponding author.
E-mail addresses: kumars.mahmoodi@abo.fi (K. Mahmoodi), jari.boling@utu.fi (J. Böling), roberto.vettor@napa.fi (R. Vettor).

https://doi.org/10.1016/j.jii.2026.101075
Received 19 September 2025; Received in revised form 9 January 2026; Accepted 16 January 2026
Available online 17 January 2026

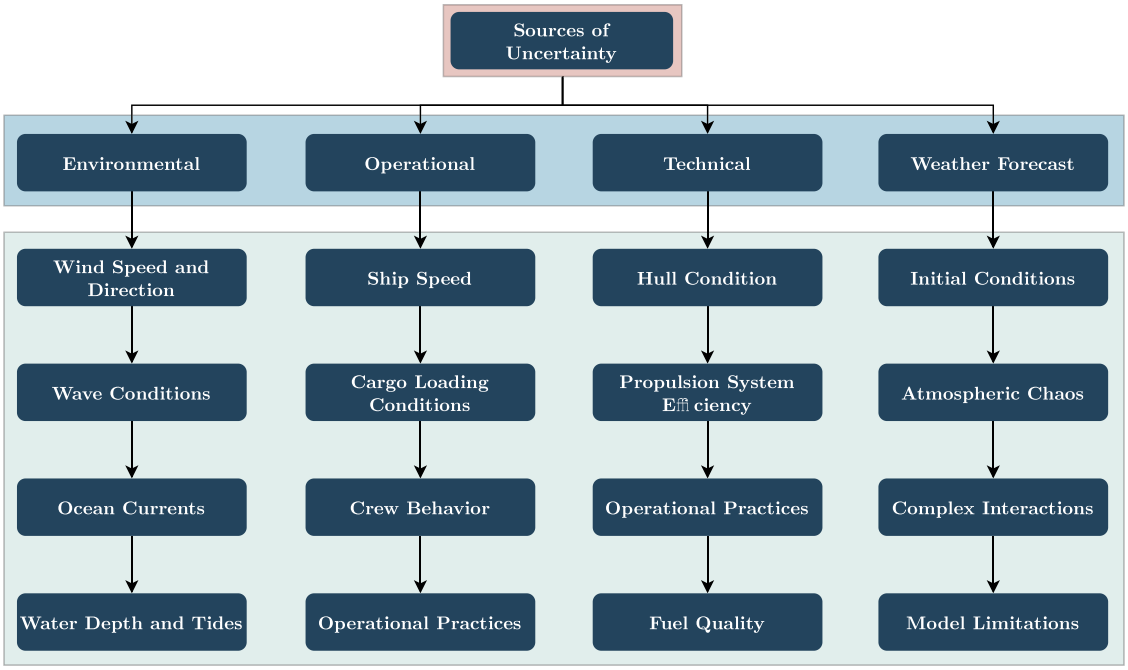

Fig. 1. Different sources of ship fuel consumption uncertainties.

the uncertainties. Hull fouling or degradation over time affects hydrodynamic efficiency [7]. Uncertainties in engine performance and propeller efficiency contribute to variations in fuel use. Variability in fuel composition and quality can influence combustion efficiency. Weather forecast uncertainties are another important source of fuel consumption uncertainties. Imperfections in weather forecasts introduce uncertainty in route planning and fuel estimation.

Enhancing the ship's operational efficiency — covering route planning, speed adjustment, and trim optimization — serves as a practical approach to reduce operating expenses and greenhouse gas emissions without necessitating any physical alterations to the vessels [8]. Various advanced algorithms have been developed to optimize the route of ships and address the complexities of route planning. Among the available strategies, the adjustment of the navigation route and the speed of the vessel represent an efficient and direct approach to minimizing operational costs during the voyages. The challenge of incorporating meteorological factors into these navigational decisions is formally recognized as the weather routing problem. Previous research has explored the optimization of ship routes and speeds, focusing on strategies to enhance fuel efficiency, reduce greenhouse gas emissions, and minimize operational costs. Such studies typically assumed a constant vessel speed and discretized the navigational domain into nodes and edges. This approach reformulated the route planning challenge as a directed graph search problem, which could then be addressed using algorithms such as Dijkstra, A*, dynamic programming, and other evolutionary and metaheuristic methodologies.

Traditional weather routing methods typically depend on deterministic weather forecasts. These forecasts, while useful, do not take into account the intrinsic uncertainties that accompany marine weather systems. Relying on a single, predicted path can lead to suboptimal routing decisions, especially in a dynamic marine environment. Marine weather is influenced by a multitude of factors, including wind patterns, ocean currents, and temperature variations that can change rapidly. This volatility requires a more sophisticated approach to weather routing. Recent advancements in numerical weather prediction have enabled the development of ensemble forecasts, which provide probabilistic insights by generating multiple realizations of potential future weather conditions. Ensemble forecasting offers a powerful means to quantify and incorporate weather uncertainties in ship routing strategies. By leveraging these probabilistic datasets, it is possible to develop more robust routing solutions that balance multiple objectives, such as fuel efficiency, safety, and adherence to schedules, under uncertain environmental conditions.

The primary aim of this study is to propose an efficient multi-objective ship weather routing strategy that incorporates uncertainties in weather parameters to minimize fuel consumption, minimize deviation from the expected estimated time of arrival (just-in-time arrival), and minimize route roughness (heading changes) for navigational stability. To this end, ensemble marine weather parameters from multiple weather data sources are collected and utilized for the route points considered in this study. These include key variables such as wind speed and direction, wave height, and ocean temperature. To solve the complex multi-objective optimization problem, this research employs the GWO method [9,10], a meta-heuristic algorithm particularly well-suited for handling multiple conflicting objectives. The proposed framework in this research simultaneously optimizes both the ship's route and its speed profile, ensuring a balanced trade-off between fuel consumption and timely arrival.

The GWO has demonstrated strong performance in solving complex, nonlinear, and constrained optimization problems across diverse domains, including coverage and connectivity maximization in wireless sensor networks [11], hierarchical multi-step energy systems optimization [12], and self-recovery regulation of rotor unbalance vibration systems [13]. These applications highlight the algorithm's robust balance between exploration and exploitation, low parameterization, and suitability for high-dimensional decision spaces. Compared to single-agent optimization algorithms such as the memorizable smoothed functional algorithm [14], safe experimentation dynamics [15], and norm-limited SPSA [16], multi-agent methods like GWO typically incur higher computational cost. However, single-agent approaches are often prone to premature convergence and reduced robustness in highly nonlinear, multi-modal, and constrained problems.

In the context of ship weather routing under uncertain environmental conditions, the population-based nature of GWO provides improved solution diversity and resilience against local optima, which outweighs the moderate increase in computational effort.

The key contributions of this study are the development of an ensemble-based multi-objective ship weather routing framework that explicitly incorporates weather uncertainty, the simultaneous optimization of route geometry and vessel speed under realistic navigational constraints, and the integration of stochastic objective aggregation within a population-based metaheuristic optimization scheme.

The rest of the paper is organized as follows. In the next section, a detailed survey of existing ship routing methods is provided. Section 3 details the problem formulation, including the proposed framework, the definition of feasible navigational areas, route formulation, assignment of ensemble weather conditions to route waypoints, constraints, multi-objective formulations, and the incorporation of ensemble weather data into the cost functions. This section also outlines the use of bootstrapping for ensemble generation. Section 4 introduces the datasets used in this study, including the onboard ship performance data, details of the selected ship voyage case studies, and the marine weather data sources. Section 5 describes the neural network model used for predicting ship fuel consumption, including the Bayesian hyperparameter optimization employed for model tuning. Section 6 provides the implementation of the GWO for solving the optimization problem. Section 7 presents the results and discusses the findings from the various objective strategies applied to different voyages. Finally, Section 8 summarizes the key contributions and insights of this work and suggests potential directions for future research.

Beyond weather-induced delays, the domain of ship schedule recovery encompasses a wide array of operational disruptions, including port congestion, equipment failures, and uncertain traffic conditions. Recent literature has extensively addressed the Vessel Schedule Recovery Problem (VSRP) through various reactive strategies such as speed adjustment, port skipping, and port swapping. For instance, study [17] focused on the coordination of vessels and ship loaders in bulk ports, proposing disruption management strategies to mitigate the impact of mechanical failures on cargo handling efficiency. Similarly, study [18] applied robust optimization to handle uncertain arrival and departure times in port traffic scheduling. The complexity of these recovery decisions often necessitates multi-objective frameworks that balance operational costs with service reliability; research [19] developed an epsilon-constraint-based approach to navigate the trade-offs between profit loss and late arrivals. Furthermore, contemporary recovery models increasingly integrate environmental sustainability. Study [20] examined recovery plans under emissions trading systems, while works [21,22] incorporated voluntary speed reduction zones and greenhouse gas limits into their optimization models. Advanced methodological approaches have also emerged, ranging from dynamic event-triggered model predictive control [23] to reinforcement learning-enhanced scheduling [24], demonstrating the industry's shift towards more adaptive and intelligent disruption management systems.

2. Literature review

Traditional ship weather routing approaches were largely deterministic and focused on shortest-path or minimum-time solutions under simplified environmental assumptions. Subsequently, modern optimization techniques such as dynamic programming, genetic algorithms, and particle swarm optimization have been introduced to improve routing performance. Most of these studies, however, addressed single-objective formulations, typically minimizing fuel consumption or voyage time independently. More recently, multi-objective ship routing frameworks have emerged to handle conflicting operational goals, though many still rely on deterministic weather inputs and limited uncertainty treatment. Paper [25] provided a taxonomy and survey of ship weather routing, which aimed to find the optimal path and sailing speed for a voyage considering environmental conditions. A modified version of Dijkstra's algorithm with heuristics, applied recursively to find the optimal route was presented in [26] using historical ship performance data and current weather conditions. In study [27], an improved cell-based method was employed to optimize the route and speed of the ship, incorporating the ECA regulations and the weather conditions. A mathematical model was developed to address the ship routing and bunker management problem using a hybrid algorithm that combines particle swarm optimization and variable neighborhood search [28].

A weather routing system was developed in study [29] using the A-star algorithm, with a modified cost function integrating oceanic and atmospheric data, three optimization objectives (shortest distance, shortest time, minimal fuel consumption), and an avoidance algorithm to exclude unsafe areas from navigation solutions. The paper [30] presented a coordinated approach based on dynamic programming to optimal voyage planning and multi-objective energy management for an all-electric ship with a hybrid energy storage system, in order to optimize the vessel route, operation cost, emissions, and energy storage degradation. A software called SIMROUTE used the A* path finding algorithm was introduced in [31] to optimize sailing routes based on wave action, utilizing Copernicus Marine Environment Monitoring Service (CMEMS) wave prediction data. An improved fractional-order particle swarm optimization algorithm was proposed [32] to optimize ship weather routing for minimum fuel consumption and maximum profit. The Non-Dominated Sorting Genetic Algorithm III (NSGA-III) was employed in [33] for multi-objective optimization. Ship operational parameters, such as heading angle and speed, were directly incorporated as optimization variables. Research [34] employed a route optimization method that integrated weather conditions and carbon emissions, utilizing a convolutional neural network to model maritime conditions and an A* guiding DDQN (A-DDQN) approach to improve navigation efficiency while minimizing randomness.

In general, research conducted on weather ship routing while considering uncertainty is limited. However, recent research has tackled the challenge of uncertainty in ship fuel consumption and other associated factors. These studies aim to improve the accuracy and reliability of predictions. Research [35] discussed advancements in ocean environmental data and models, focusing on uncertainties in wind, waves, currents, sea levels, and ice. Paper [36] categorized sources of uncertainty in ship performance monitoring and presented a method to quantify these uncertainties. In [37], a probabilistic approach was used to quantify how weather conditions' uncertainties affect a vessel's fuel consumption. A study by the International Maritime Organization (IMO) on the uncertainty of different methods for measuring the annual consumption of fuel oil of ships is discussed in [38]. Research [39] explored the accuracy of fuel consumption predictions for ships using a generic energy systems model for a RoRo ship and a tanker. It categorized and handled uncertainties across four phases of a ship's life, from design to operation. The research paper [40] used numerical probability simulations and grey relational analysis to study the impact of various factors and weather conditions on fuel consumption. This method showed a 27.5% reduction in fuel oil consumption and a significant drop in the Efficiency Operational Indicator (EEOI) index. Study [2] explored methods to predict ship fuel consumption uncertainties along specific routes using ensemble weather forecasts. It compared a brute-force approach with probabilistic methods, showing reasonable agreement for a containership's North Atlantic passage.

A methodology to quantify the impact of numerical error and performance model uncertainty on weather routing predictions is presented in [41]. Applied to a Polynesian voyaging canoe, it found that numerical error is significantly smaller than performance model uncertainty which highlights the importance of considering both factors in weather routing studies. Study [42] highlighted that weather uncertainties and ship performance models significantly impact voyage optimizations. It

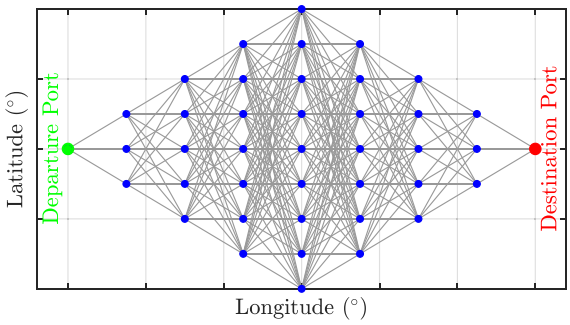

Fig. 2. An example of a discretized network of possible sailing paths for the route optimization purpose.

proposed a speed optimization method for voluntary speed reduction, which proved more effective than course optimizations for long voyages in harsh weather. Study [43] defined probabilistic objectives and constraints for route optimization systems, incorporating weather-related uncertainties through ensemble forecasts. It used classical reliability methods to evaluate the probability of failure and variability in predicted fuel consumption and arrival times for a major North Atlantic route. Study [44] developed two robust optimization models using bounded and budget-bounded uncertainty sets to address the liner ship routing and scheduling problem under uncertain weather and ocean conditions. The research [45] introduced an enhanced evolutionary multi-objective weather routing method for ships with incorporating uncertainties in weather forecasts. By leveraging the w-MOEA/D algorithm, it optimized routes based on decision maker's preferences under various constraints and uncertainties. Moreover, a comprehensive view of uncertainties in maritime ship routing and scheduling is provided in [46]. It highlighted critical gaps and offered recommendations for researchers, emphasizing the importance of addressing uncertainties in travel times, port handling times, demand, and fuel prices to improve decision-making in maritime transportation. This paper [47] reviewed the path planning algorithms used in autonomous maritime surface ships, focusing on the navigation safety perspective and the challenges of implementing these algorithms in a complex and dynamic maritime environment. A modified probabilistic roadmap algorithm was developed [48] to solve the ship weather routing problem, utilizing random sampling across the navigation area, a graph-based roadmap with weighted paths reflecting sea region weather conditions, and a modified Dijkstra's algorithm to optimize the route based on fuel consumption and travel time. The paper [49] provided an overview of ship performance models and ice routing algorithms for Arctic weather routing, identifies limitations of existing approaches, and proposes a dynamic multi-objective path planning algorithm (D*-NSGA-III) to address the challenges of the rapidly changing Arctic environment.

3. Problem formulation

Ship weather routing is a complex optimization problem that involves determining the most suitable navigational path and speed profile for a vessel, considering a wide range of dynamic and uncertain environmental conditions. The key objective is to find an optimal balance among multiple conflicting criteria such as minimizing fuel consumption and ensuring arrival within a designated time window. Achieving this balance is particularly challenging due to the stochastic nature of marine weather conditions, including wind, waves, and ocean currents. Fig. 2 illustrates an example of a discretized network of possible sailing paths, where each node represents a feasible position a ship might occupy during its voyage at a given time interval. The interconnected blue nodes represent candidate waypoints, and the gray lines show all possible transitions a vessel may take from one waypoint to the next.

The general framework proposed for this study is shown in Fig. 3. Moreover, Table 1 provides the nomenclature adopted in this study, listing all key variables and parameters used in the proposed optimization framework. The proposed framework integrates ship operational data, ensemble weather forecasts, and optimization techniques to develop a robust methodology for multi-objective ship weather routing under uncertainty. The process begins with collecting onboard voyage performance data, including timestamps, positions (latitude and longitude), ship speed, and fuel consumption, as well as relevant meteorological and oceanographic parameters of a case study ship during a voyage. This onboard dataset is integrated with external, high-resolution datasets such as ECMWF or MFWAM. A machine learning-based predictive model for ship fuel consumption is developed using a multilayer perceptron (MLP) architecture, whose structure and hyperparameters are tuned using Bayesian optimization. The MLP receives selected ship and environmental parameters as inputs and predicts fuel consumption as output. This model is then used to estimate the fuel usage for candidate voyage routes under varying weather conditions.

The geographical domain between the departure and destination ports is discretized into a grid-based network of feasible cells. Obstacle regions such as islands, land, or shallow water zones (identified using GEBCO bathymetry) are excluded from the feasible set. Each candidate route is then discretized into a sequence of segments characterized by decision variables: the heading angle between successive nodes, the ship speed for each segment, and the time duration for each segment. For each segment of a candidate route, ensemble-based weather parameters (from multiple forecast members) are extracted. Weather data are assigned by averaging the values from nearby recognition points surrounding each segment's center. The ensemble provides multiple realizations of weather conditions, which enables a stochastic evaluation of the route's performance under uncertainty.

The route optimization is formulated as a multi-objective, constrained optimization problem. A set of safety, navigational, and performance-based constraints is enforced, including maximum heading change, speed limits, obstacle avoidance, bathymetric depth, and maximum tolerable wave and wind conditions. The objectives include minimizing total fuel consumption, achieving just-in-time arrival, and improving route smoothness. Each candidate route is evaluated against all ensemble members, and objectives are aggregated using a stochastic optimization strategy that minimizes the expected objectives across scenarios. The outcome is a robust, ensemble-aware optimal route and speed profile tailored to varying weather conditions and operational constraints.

In the context of ship weather routing, relying on a single-objective optimization model can result in suboptimal operational decisions, particularly when complex environmental uncertainties are involved. For example, minimizing only sailing time may guide the vessel through regions with high wave activity or strong adverse winds, which could lead to increased fuel consumption and emissions due to greater resistance and power demands. Conversely, optimizing solely for fuel efficiency might favor longer routes that bypass challenging weather zones, which can extend voyage duration and conflict with just-in-time arrival requirements. These trade-offs highlight the limitations of single-objective approaches and underscore the need for a multi-objective framework that balances operational costs, emissions, and schedule adherence while incorporating weather variability through ensemble forecasts.

3.1. Define feasible navigational area

In order to define the admissible search space for ship routing, the maritime domain between the departure and destination ports is discretized into a two-dimensional grid consisting of uniformly spaced cells (Fig. 4), each corresponding to a specific geographical location

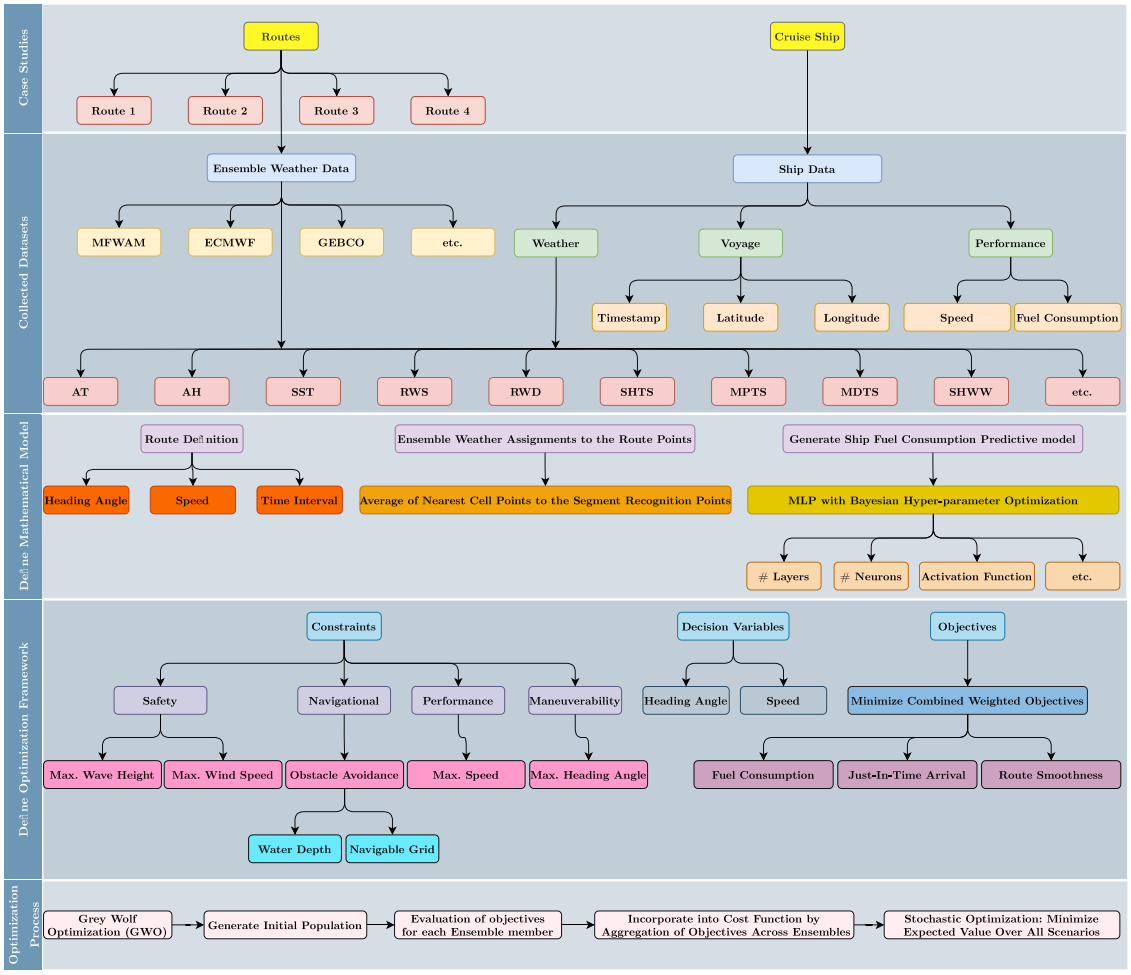

Fig. 3. The proposed framework for this study.

characterized by its latitude and longitude. This grid-based representation provides a structured environment in which the connectivity and feasibility of candidate paths can be efficiently evaluated.

Rather than relying on water depth as a limiting factor, the feasibility of each grid cell is determined based on the presence of static geographical obstacles such as islands, landmasses, and restricted navigation zones. These obstacles are identified using geospatial data and are geometrically represented as closed polygons within the routing domain. A binary navigability mask is applied across the grid, where each cell is assigned a value based on whether it lies inside or outside the defined obstacle regions:

$$\text{Feasibility}(x,y) = \begin{cases} 0, & \text{if } (x,y) \notin \text{Obstacle Region} \quad \text{(navigable)} \\ 1, & \text{if } (x,y) \in \text{Obstacle Region} \quad \text{(non-navigable)} \end{cases} \tag{1}$$

This binary feasibility map effectively partitions the domain into navigable and non-navigable regions. Cells intersecting any portion of the obstacle polygons are marked as infeasible (1), while all remaining cells are considered viable for routing (0). In this study, a computational approach is developed to recognize navigational and non-navigational areas automatically without direct user involvement, leveraging geospatial data and MATLAB's Mapping Toolbox. Natural Earth coastline data, accessible through the Mapping Toolbox, is employed to distinguish land and water features. Each grid point is classified as navigational or non-navigational using a point-in-polygon algorithm. Fig. 5 shows the output of the considered approach for the entire world. In this figure, navigational and non-navigational areas are shown with blue and red colors, respectively.

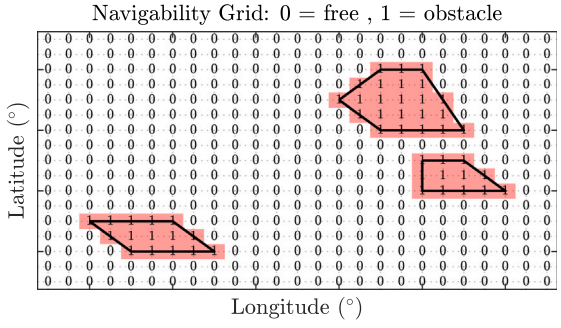

Fig. 4. An example of discretizing the navigational area to feasible and infeasible cell grids.

3.2. Route definition

In this study, the considered ship route is defined as a sequence of spatially discretized waypoints connecting the departure and destination ports. The geographical area is first divided into a grid of feasible cells, in which the vessel is allowed to navigate only through cells that satisfy obstacle avoidance. The routing domain is discretized such that each feasible path corresponds to a sequence of segments indexed by $k = 1, 2, \ldots, K$, where K is the number of segments in the route.

Fig. 6 shows the method for generating route waypoints. Each waypoint is denoted by its geographical coordinates $\mathbf{P}_k = [\varphi_k, \lambda_k]$,

Table 1
Nomenclature of the main variables and parameters used in the proposed optimization framework.

Symbol	Description
K	Total number of route segments (waypoints)
k	Index for route segment, $k = 1, \dots, K$
M	Number of ensemble weather forecast members
m	Index for ensemble member, $m = 1, \dots, M$
N	Number of search agents (wolves) in GWO
i	Index for search agent, $i = 1, \dots, N$
t	Current iteration number
(x_k, y_k)	Latitude and longitude of route waypoint at segment k
$\mathbf{P}_k$	Position vector of the ship at route segment k
θ_k	Ship heading angle at segment k (measured clockwise from true north)
v_k	Ship speed at segment k
Δt_k	Travel time of route segment k
T_{ETA}	Estimated time of arrival
T_{target}	Target arrival time
$\Delta\theta_{\max}$	Maximum allowable heading angle change between segments
$v_{\min}, v_{\max}$	Minimum and maximum allowable ship speeds
$d(x, y)$	Water depth at location (x, y)
$d_{\min}$	Minimum allowable water depth (draft plus safety margin)
$H_s(x, y, t)$	Significant wave height at location (x, y) and time t
$W_s(x, y, t)$	Wind speed at location (x, y) and time t
$H_{s,\max}$	Maximum allowable significant wave height
$W_{s,\max}$	Maximum allowable wind speed
Feasibility(x, y)	Binary navigability indicator of grid cell (x, y)
M	Number of ensemble members
$J^{(m)}$	Objective function value for ensemble member m
$\mathbb{E}[J]$	Expected objective value over ensemble members
J_{fuel}	Fuel consumption objective
J_{time}	Just-in-time arrival objective
J_{smooth}	Route smoothness objective
w_1, w_2, w_3	Weights of fuel, time, and smoothness objectives
N	Number of search agents (wolves) in GWO
α, β, δ	Best three solutions in the Grey Wolf Optimizer
$\vec{A}, \vec{C}$	GWO control coefficient vectors
a	Linearly decreasing parameter controlling exploration–exploitation

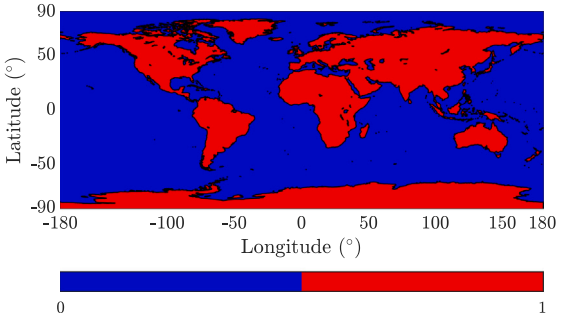

Fig. 5. Discretizing the world areas to feasible and infeasible cell grids with an automatically implemented approach.

where φ_k and λ_k denote the latitude and longitude at the kth segment, respectively. The vessel's motion from one waypoint to the next is governed by the heading angle θ_k and speed v_k, which are considered as decision variables in the optimization problem. θ_k is converted to radians internally for trigonometric operations. The speed v_k is expressed in knots, and multiplied by a degree-per-knot-hour scaling factor ($\approx$0.01667) to convert distance traveled into angular displacement in latitude and longitude. The time interval required to travel between waypoints k and $k+1$ is defined as Δt_k, which is calculated based on the traveled distance and the ship speed. The heading angle and speed remain consistent between two waypoints, with a constant sailing time interval between adjacent waypoints.

Assuming the heading angle θ_k is measured clockwise from true north (in line with maritime convention), the vessel's position at the next waypoint can be computed using the following kinematic equations:

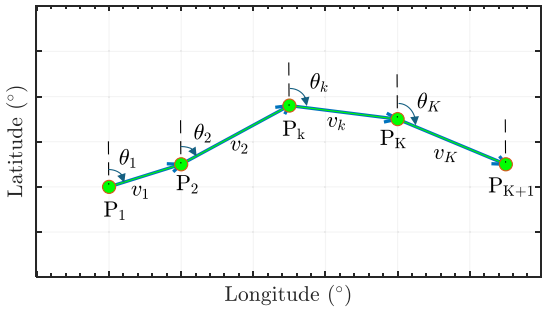

Fig. 6. Considered approach for generating route waypoints in the optimization process.

$$x_{k+1} = x_k + v_k \cdot \Delta t_k \cdot \sin(\theta_k), \tag{2}$$

$$y_{k+1} = y_k + v_k \cdot \Delta t_k \cdot \cos(\theta_k). \tag{3}$$

or, in vector form:

$$\mathbf{P}_{k+1} = \mathbf{P}_k + v_k \cdot \Delta t_k \cdot \begin{bmatrix} \sin(\theta_k) \\ \cos(\theta_k) \end{bmatrix}, \text{ for}(k = 1, 2, \dots, K) \tag{4}$$

Overall, the route is represented as a sequence of $(\theta_k, v_k, \Delta t_k)$ triplets, and the optimization algorithm seeks to determine the optimal set of these variables. To ensure navigational feasibility and realism:

- Heading angle changes between successive segments are limited to $\Delta\theta_{\max} = 30°$ (except for encountering obstacles) to account for ship maneuvering constraints.
- Ship speed is bounded within a practical operational range $v_k \in [5, 20]$ knots.
- Both the initial and final segments are treated as standard segments with constrained speed, but are not explicitly modeled with acceleration or deceleration phases. This simplification is justified given the hourly time-step resolution.

To guide the route toward the destination while respecting maneuvering limits, the target heading angle θ_k is initialized using the great-circle bearing between the current position and the destination port. This bearing is computed using the following formula:

$$\theta_k = \text{atan2}\left(\sin(\Delta\lambda)\cos(\varphi_{\text{dest}}),\ \cos(\varphi_k)\sin(\varphi_{\text{dest}}) - \sin(\varphi_k)\cos(\varphi_{\text{dest}})\cos(\Delta\lambda)\right) \tag{5}$$

where $\Delta\lambda = \lambda_{\text{dest}} - \lambda_k$, and φ_{dest}, λ_{dest} represent the latitude and longitude of the destination. This target heading is then adjusted within a specified maneuvering range to introduce variability and ensure feasible trajectory generation.

Finally, the proposed framework checks whether each segment passes through any forbidden zone (obstacles) by sampling multiple points along the segment and verifying their location against a predefined navigability grid. If any sampled point lies inside an obstacle, the segment is discarded and re-sampled to guarantee full obstacle avoidance during route generation.

3.3. Ensemble weather assignments to the route waypoints

Weather and sea state parameters, which are spatio-temporally varying and uncertain, are assigned to each route segment using the average of surrounding recognition points from ensemble forecasts. The concept of this approach is shown in Fig. 7. In this figure, the route segment is defined by two endpoints, along which several weather grid nodes (spatial grid, e.g., ERA5 or ECMWF data) with random values are

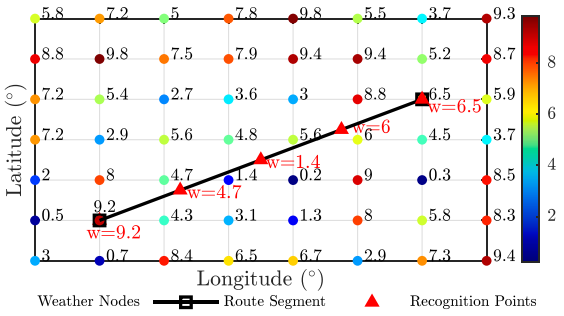

Fig. 7. Considered approach for assigning ensemble weather parameters to the route segments.

dispersed. Recognition points are located along the route segment (in this figure, 5 triangular points). Each recognition point gets assigned the nearest weather node value. Then, the average weather value will be calculated based on the overall average of the weather values of the recognition point. Therefore, the weather value of the considered segment in Fig. 7 is the average of values 9.2, 4.7, 1.4, 6, and 6.5, which is 5.56. This process will be repeated for each ensemble member of the considered weather parameter.

3.4. Constraints

The ship routing optimization problem is subject to a variety of physical and operational constraints to ensure feasible, safe, and efficient voyages. These constraints are grouped into four major categories: Safety, Navigational, Performance, and Maneuverability constraints, each defined based on operational requirements and environmental conditions along the candidate routes.

Safety constraints are imposed to prevent the vessel from navigating through hazardous sea states. Specifically, thresholds are set on the significant wave height and wind speed to reflect operational safety limits of the ship:

$$H_s(x, y, t) \leq H_{s,\max} \tag{6}$$

$$W_s(x, y, t) \leq W_{s,\max} \tag{7}$$

where $H_s(x, y, t)$ is the significant wave height and $W_s(x, y, t)$ is the wind speed at grid cell (x, y) and time t. $H_{s,\max}$ and $W_{s,\max}$ represent ship-specific upper limits beyond which navigation is considered unsafe.

Navigational constraints enforce that the ship only traverses accessible and legal water regions. These constraints are implemented through: Obstacle avoidance and Water depth restriction. Obstacle avoidance, ensuring that no route segment intersects any predefined static obstacle (e.g., islands or restricted zones). Each cell (x, y) has an associated binary feasibility value as mentioned in Eq. (1). All candidate routes must only include cells for which $\chi(x, y) = 1$. The water depth restriction can be included to ensure that navigation occurs only in cells with sufficient bathymetric clearance. This can be formulated as:

$$d(x, y) \geq d_{\min} \tag{8}$$

where $d(x, y)$ is the water depth and $d_{\min}$ is the vessel's draft plus safety margin.

Performance constraints limit the vessel's operating envelope, particularly with respect to its speed:

$$v_k \leq v_{\max}, \quad \forall k \tag{9}$$

where v_k is the vessel speed at route segment k and $v_{\max}$ is the maximum allowable speed due to engine limits, sea state, or efficiency considerations.

Maneuverability constraints are defined to restrict rapid or infeasible changes in the ship's heading direction. The change in heading angle between consecutive route segments is limited by:

$$|\theta_{k+1} - \theta_k| \leq \Delta\theta_{\max}, \quad \forall k \tag{10}$$

where θ_k is the heading angle at segment k and $\Delta\theta_{\max}$ is the ship's maximum allowable turn angle, ensuring smooth and physically realizable trajectories.

To ensure that the vessel arrives at the destination port within a required time window, an arrival time constraint is incorporated into the optimization framework. The estimated time of arrival, denoted as T_{ETA}, is computed as the cumulative sum of the travel times over all route segments. Given a predefined target arrival time T_{target}, the constraint is expressed as:

$$T_{\text{ETA}} \leq T_{\text{target}} \tag{11}$$

These constraints collectively define the feasible solution space within which the optimization algorithm searches for optimal ship routes. Each constraint reflects either environmental limitations, ship design capabilities, or safety standards, and is dynamically evaluated along potential routes using spatio-temporal environmental datasets.

3.5. Objectives

The ship weather routing problem is formulated as a multi-objective optimization problem. The objective is to determine the optimal set of decision variables, namely the vessel's heading angles and speeds at each segment of the route, such that a combination of operational and environmental goals is achieved.

Decision Variables:

- θ_k: Heading angle at the kth segment.
- v_k: Vessel speed at the kth segment.

These variables are optimized over the full route with the aim to minimize a weighted combination of three primary objectives:

1. Fuel Consumption (J_{fuel})
2. Just-in-Time Arrival (J_{time})
3. Route Smoothness (J_{smooth})

The overall objective function is formulated as a weighted sum:

$$\min_{\theta_k, v_k} \quad J = w_1 J_{\text{fuel}} + w_2 J_{\text{time}} + w_3 J_{\text{smooth}} \tag{12}$$

where w_1, w_2, and w_3 are user-defined non-negative weights satisfying $w_1 + w_2 + w_3 = 1$.

The total fuel consumption along the route depends on weather conditions and ship speed. A machine learning-based model $F(v_k, \vec{e}_k)$ is used, where $\vec{e}_k$ denotes environmental inputs (e.g., wind, waves):

$$J_{\text{fuel}} = \sum_{k=1}^{N} F(v_k, \vec{e}_k) \cdot \Delta t_k \tag{13}$$

where $\Delta t_k = \frac{d_k}{v_k}$ is the travel time for segment k, and d_k is the length of the segment.

To promote arrival at a target time T_{target}, the actual estimated time of arrival T_{ETA} is calculated as:

$$T_{\text{ETA}} = \sum_{k=1}^{N} \Delta t_k = \sum_{k=1}^{N} \frac{d_k}{v_k} \tag{14}$$

The just-in-time arrival penalty is defined as:

$$J_{\text{time}} = \left| T_{\text{target}} - T_{\text{ETA}} \right| \tag{15}$$

To avoid zig-zagging routes and ensure maneuverability, the change in heading angle between consecutive segments is penalized:

$$J_{\text{smooth}} = \sum_{k=1}^{N-1} (\theta_{k+1} - \theta_k)^2 \tag{16}$$

Squaring in the smoothness objective gives more weight to larger changes in heading angles. This is useful because abrupt course changes are more undesirable (in terms of safety, fuel, and comfort) than mild deviations. This promotes smoother, more navigable paths, reducing steering effort and improving fuel efficiency.

Together, these objectives form a flexible framework capable of addressing the core requirements in ship route planning. By tuning the weights (w_1, w_2, w_3), different operational priorities (e.g., economy vs. punctuality vs. maneuverability) can be reflected in the optimization process.

In this study, a weighted sum aggregation method is adopted instead of a Pareto-based multi-objective approach (e.g., MOGWO). This choice is motivated by the operational need for a single, actionable route recommendation based on pre-defined preferences (e.g., fuel prices and charter schedules), rather than requiring the operator to select from a set of trade-off solutions in real-time. Furthermore, given the high computational cost of evaluating stochastic objective functions (e.g., CVaR) across large ensemble datasets, the weighted sum method offers a computationally efficient solution that ensures faster convergence while effectively reflecting the decision-maker's priorities.

3.6. Incorporate ensemble members into cost function

To account for weather uncertainties, the performance of each candidate route is evaluated over all ensemble weather members, and the aggregated objective value is computed as the expected cost across ensemble realizations. Instead of relying on a single deterministic weather forecast, ensemble data from multiple weather model realizations are used to represent possible environmental scenarios. For each candidate route, the objective function is evaluated under all ensemble members, and the aggregated objective is computed as the expected value of these evaluations.

Let $J^{(m)}$ denote the cost of a route under ensemble member m, where $m = 1, 2, \ldots, M$. Different strategies are adopted to incorporate ensemble information into the overall cost function:

3.6.1. Mean approach

The most common strategy is to minimize the expected value of the cost across all ensemble members:

$$\mathbb{E}[J] = \frac{1}{M} \sum_{m=1}^{M} J^{(m)} \tag{17}$$

This approach aims to achieve good average performance across the range of possible realizations.

3.6.2. Worst-case approach

To ensure robustness against the most adverse weather conditions, the cost can be defined based on the maximum cost among all ensemble members:

$$J_{\text{worst}} = \max_{m=1,\ldots,M} J^{(m)} \tag{18}$$

This conservative strategy minimizes the impact of the worst-case scenario.

3.6.3. Risk-aware (mean–variance) approach

A risk-averse objective can be formulated by penalizing variability among ensemble members. A common formulation combines the expected cost and its standard deviation:

$$J_{\text{risk}} = \mathbb{E}[J] + \lambda \, \text{std}(J) \tag{19}$$

where λ is a risk-aversion weighting parameter controlling the balance between mean performance and variability. It controls the trade-off between minimizing the expected cost and reducing the variability (uncertainty) associated with the outcome. A higher value of λ places greater emphasis on reducing the standard deviation of the cost across ensemble members, thereby promoting more conservative and robust solutions. Conversely, a lower λ prioritizes optimizing the mean performance while accepting higher variability. The choice of λ reflects the decision-maker's tolerance for risk and uncertainty in route planning under stochastic environmental conditions.

3.6.4. Conditional value-at-risk approach

Another risk-focused method is the CVaR, which aims to minimize the expected cost among the worst $\alpha\%$ scenarios:

$$\text{CVaR}_{\alpha}(J) = \mathbb{E}\left[J \mid J \geq \text{VaR}_{\alpha}(J)\right] \tag{20}$$

where $\text{VaR}_{\alpha}(J)$ denotes the Value-at-Risk at a given confidence level α. This approach concentrates on controlling the tail risk. $\text{CVaR}_{\alpha}(J)$ captures the average cost among the worst $(1-\alpha)100\%$ of cases. The selection of the confidence level α (typically between 90% and 99%) reflects the level of risk tolerance. A higher α (e.g., 0.99) focuses on even rarer but more catastrophic events, leading to highly conservative but safer solutions.

In the context of ship route optimization under ensemble-based weather uncertainty, applying CVaR allows the optimizer to generate solutions that are not only good on average but also resilient against the worst realizations of environmental conditions. Particularly for critical maritime operations, where extreme weather events can significantly impact fuel consumption, travel time, and safety, incorporating CVaR into the cost function leads to more robust and practical route planning.

3.6.5. Bootstrapping method for ensemble generation

In ensemble-based ship weather routing, data from multiple sources are integrated to generate optimal voyage predictions. However, due to inconsistencies in data availability, some variables may have fewer ensemble members than others. This imbalance can lead to errors in calculating the objective function, as uniform ensemble sizes across all variables are required for accurate probabilistic modeling.

To ensure statistical consistency and fair evaluation across ensemble members, this study adopts a bootstrapping strategy to generate a uniform ensemble set. Rather than discarding ensemble members or performing arbitrary interpolation, the bootstrapping approach resamples available data using sampling with replacement. This process is repeated across all relevant variables and route segments, resulting in a complete and coherent ensemble member. Fig. 8 illustrates the concepts of the Bootstrapping method used for ensemble generation in this study. It illustrates how different weather variables, initially having inconsistent ensemble members, are balanced by generating multiple ensemble sets. In this figure, for instance, three variable groups (AT, RWS, and SHWW) with initially different numbers of ensemble members are given. Multiple ensemble sets $(\text{m}_1, \text{m}_2, \text{m}_3, \ldots, \text{m}_m)$ are created using Bootstrapping. Each ensemble set consists of one representative from each variable group.

The key advantage of this strategy is that it maintains the statistical variability inherent in the original data, avoids introducing bias from interpolated or assumed values, and allows the construction of a consistent ensemble of size M, even if the original datasets had unequal or sparse member distributions.

4. Collected datasets

4.1. Onboard ship performance dataset

The case study Cruise ship (Fig. 9), built in 2017, has a gross tonnage of 99,000 and a maximum speed of 21.7 knots. It is equipped with a total installed power of 48,000 kW. The ship measures 295.3 m in length overall, with a beam of 42.3 m and a draught of 8.2 m. It has a summer deadweight of 7900 tons.

A case study voyage (Fig. 10), including onboard weather and ship performance dataset, is selected for generating the considered ship fuel consumption predictive model. The voyage, taking place from

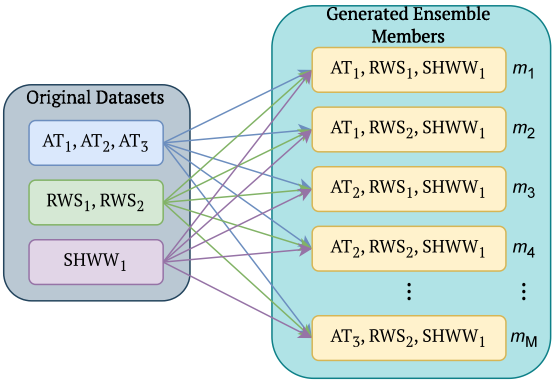

Fig. 8. The concepts of the bootstrapping method used for ensemble generation.

Fig. 9. Considered case study ship.

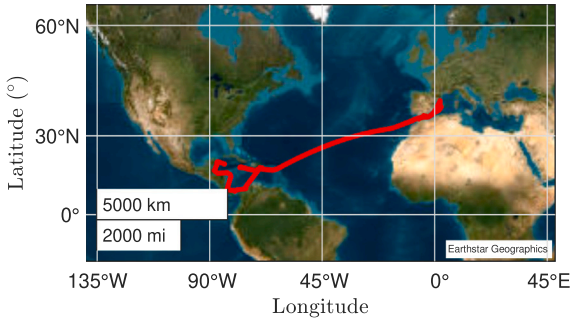

Fig. 10. Case study voyage for generating the ship fuel consumption predictive model based on onboard weather and ship performance data along the Atlantic Ocean [red line].

April 6 to April 13, 2018, crosses the Atlantic Ocean. For training the predictive model, 8961 points along this route are selected, with data sampled at one-minute intervals. The onboard data encompasses various collected variables related to the voyage, ship, and weather parameters. Route parameters include timestamps and positions (latitude and longitude) of voyage segments. Additional collected thirteen parameters are Ambient Temperature (AT), Ambient Humidity (AH), Sea Surface Temperature (SST), Relative Wind Speed (RWS), Relative Wind Direction (RWD), Significant Wave Height of Total Swell (SHTS), Mean Period of Total Swell (MPTS), Relative Swell Wave Direction (MDTS), Significant Height of Wind Waves (SHWW), Mean Period of Wind Waves (MPWW), Mean Direction of Wind waves (MDWW), Ship Speed (Speed Through Water) (STW), and Total Motors' Fuel Consumption (MFC). The visual representation of the considered variables is illustrated in Fig. 11.

4.2. Ship voyage case studies

Four hypothetical ship voyages obtained from [50] are considered to compare the effectiveness of the proposed optimization framework. The details of these voyages are presented in Table 2

4.3. Marine weather data

The marine and weather data for the route points are sourced from various providers, as detailed in Tables 3 and 4. Data are interpolated to hourly values based on the specific model used. For instance, Fig. 12 shows the combined significant height of wind and swell waves and wind speed of the voyages at the departure time obtained from the ERA5 dataset. Moreover, as an example, Fig. 13 shows the collected ensemble wind speed and significant height of wind waves for desired routes of the studied voyages. 200 points are randomly selected from each route. Moreover, the geographical maps of the selected routes are presented in Fig. 14. In this figure, the solid line indicates the mean of the ensemble members, while the shaded area surrounding it illustrates their range.

The bathymetry data are obtained from the GEBCO gridded bathymetry dataset [51]. This dataset offers comprehensive global coverage, with a spatial resolution of 15 arc-seconds which provides detailed representations of both ocean floors and terrestrial terrains.

5. Neural network model with Bayesian hyperparameter optimization

In this study, a feed-forward MLP neural network with Bayesian hyperparameter optimization [54–56] is applied to capture the nonlinear relationships between various ship and weather parameters and the resulting ship fuel consumption output. The MLP model consists of an input layer corresponding to ship operational and weather parameters (see Section 4.1). Hidden layers are structured to optimize the trade-off between model complexity and computational efficiency [57], with the number of layers and neurons determined through the Bayesian optimization process. The output layer predicts the ship's fuel consumption for a given operational condition.

A schematic diagram of a three-layer MLP neural network is presented in Fig. 15. The structure of the MLP network consists of an input layer, hidden layer(s), and an output layer. These inputs are passed to the hidden layers. The hidden layers consist of neurons that perform weighted linear combinations of the inputs followed by activation functions to introduce nonlinearity [58,59]. The final output layer, consisting of a single or multiple neurons with a linear activation function, predicts the outputs. Training is conducted using backpropagation with LBFGS [60] optimizer to minimize the loss function Mean Squared Error (MSE).

Bayesian optimization is used to fine-tune the hyperparameters of the neural network, including the number of hidden layers, neurons per layer, activation functions, iteration limit, regularization strength (Lambda), and standardized data (yes or no). It utilizes a Gaussian process [61] as a surrogate model to explore the hyperparameter space efficiently. This method explores various combinations of hyperparameter values through an optimization scheme aimed at minimizing the model's MSE, ultimately yielding a model with optimized hyperparameters. Hyperparameter optimization offers considerable benefits by systematically improving model performance and efficiency. By fine-tuning network structure parameters, the optimization process ensures that the network is neither under- nor over-parameterized which results a balance between complexity and generalization. Techniques like Bayesian optimization efficiently explore the hyperparameter space which reduces trial-and-error efforts and computational costs. The critical components in the minimization process of Bayesian optimization algorithm include [62]: a Gaussian process model of $f(x)$, a Bayesian update procedure for refining the Gaussian process model with each new evaluation of $f(x)$, and an acquisition function $a(x)$, derived from the Gaussian process model of f, which is maximized to determine the subsequent evaluation point x.

6. Grey wolf optimizer

The GWO [9,10] is a nature-inspired metaheuristic algorithm that simulates the social hierarchy and hunting behavior of grey wolves

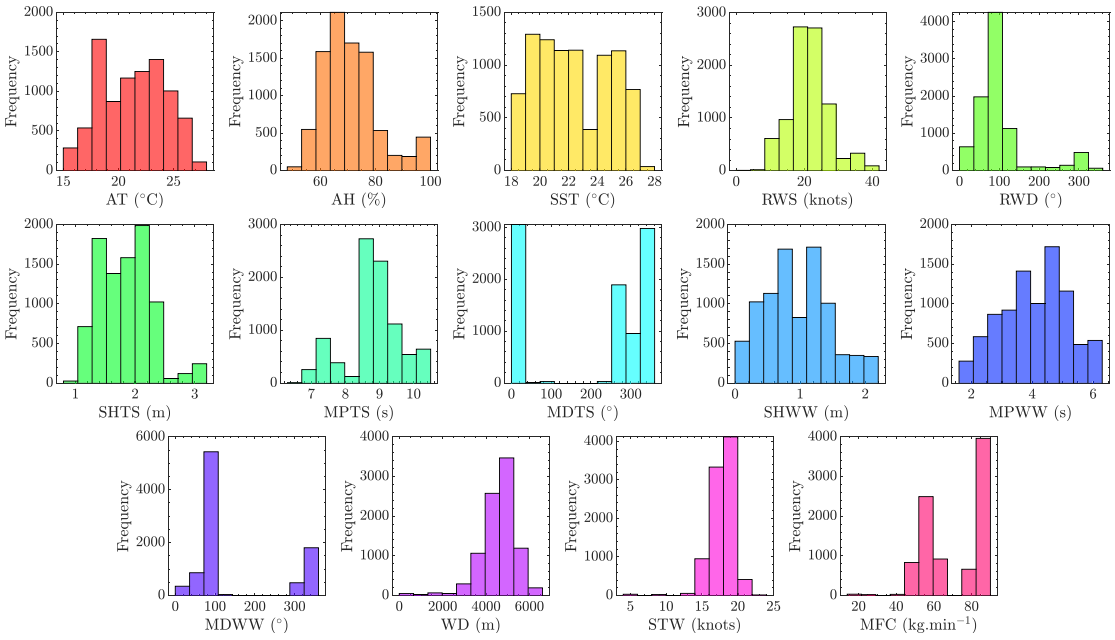

Fig. 11. Visual representation of the considered onboard weather and ship variables for generating the ship fuel consumption predictive model.

Table 2
Details of the case study ship voyages for performance evaluation of the proposed optimization framework.

Voyages	Start position	End position	Approximate distance	Depart from the port	Arrive at the port	Start date/time	End date/time
Voyage 1	N 39.632°–E 19.904°	N 45.646°–E 13.723°	1000 km	Corfu Island, Greece	Trieste, Italy	01 Oct 2023, 07:00	02 Oct 2023, 15:00
Voyage 2	N 35.359°–E 25.161°	N 28.131°–W 15.380°	4000 km	Heraklion, Crete, Greece	Las Palmas de Gran Canaria	03 Nov 2023, 22:00	9 Nov 2023, 13:30
Voyage 3	N 28.194°–W 15.399°	S 33.878°–E 18.414°	8300 km	Las Palmas de Gran Canaria	Cape Town, South Africa	12 March 2024, 22:30	27 March 2024, 14:30
Voyage 4	N 1.244°–E 103.871°	N 23.651°–E 58.581°	6000 km	Singapore	Muscat, Oman	08 May 2024, 14:00	19 May 2024, 19:30

Table 3
Sources of considered marine data variables [52,53].

Dataset	Region	Spatial resolution	Temporal resolution	Update frequency
MeteoFrance MFWAM	Global	0.08° (8 km)	3-Hourly	Every 12 h
ECMWF WAM	Global	0.25° (25 km)	3-Hourly	Every 6 h
NCEP GFS Wave	Global	0.25° (25 km)	Hourly	Every 6 h
DWD GWAM	Europe	0.05° (5 km)	Hourly	Every 12 h
DWD EWAM	Global	0.25° (25 km)	Hourly	Every 12 h
ERA5-Ocean	Global	0.5° (50 km)	Hourly	Every 24 h with 5 days delay

Table 4
Considered weather models and their features [52,53].

Weather model	National weather provider	Resolution	Forecast length	Update frequency
ICON	Deutscher Wetterdienst (DWD)	2–11 km	7.5 days	Every 3 h
GFS & HRRR	NOAA	3–25 km	16 days	Every hour
ARPEGE & AROME	Météo-France	1–25 km	4 days	Every hour
IFS & AIFS	ECMWF	25 km	7 days	Every 6 h
MSM & GSM	JMA	5–55 km	11 days	Every 3 h
MET Nordic	MET Norway	1 km	2.5 days	Every hour
HARMONIE	KNMI	2 km	2.5 days	Every hour
HARMONIE	DMI	2 km	2.5 days	Every 3 h
GEM	Canadian Weather Service	2.5 km	10 days	Every 6 h
GFS GRAPES	China Meteorological Administration (CMA)	15 km	10 days	Every 6 h
ACCESS-G	Australian Bureau of Meteorology (BOM)	15 km	10 days	Every 6 h

(Canis lupus) in nature. The algorithm has been successfully applied to a wide range of optimization problems [63–66] due to its simplicity, ease of implementation, and effective balance between exploration and exploitation [67]. Compared to other swarm intelligence algorithms

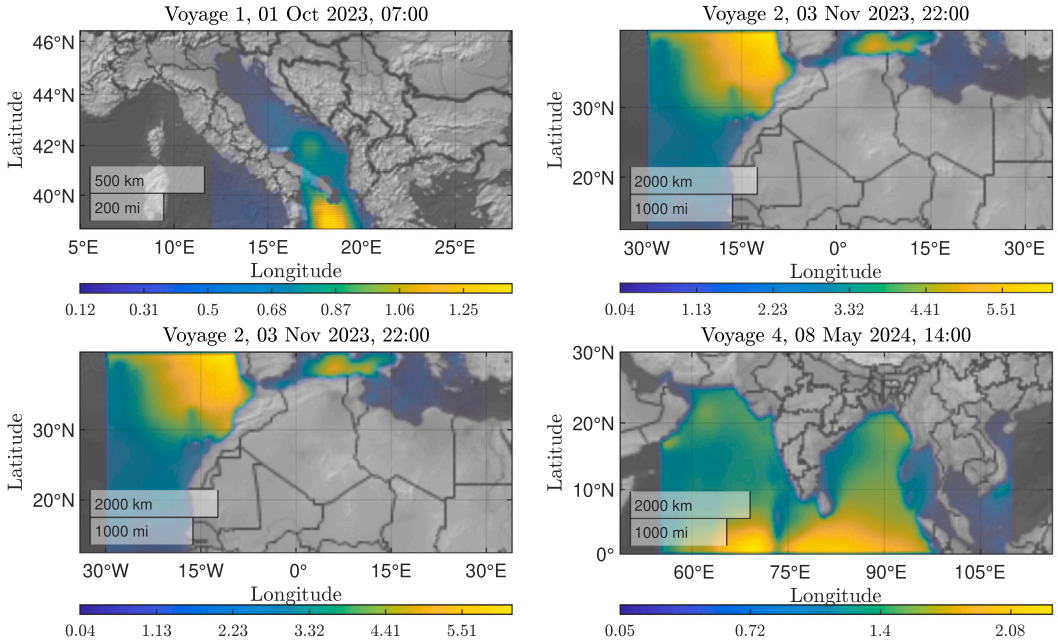

(a) Combined significant height of wind and swell waves (m)

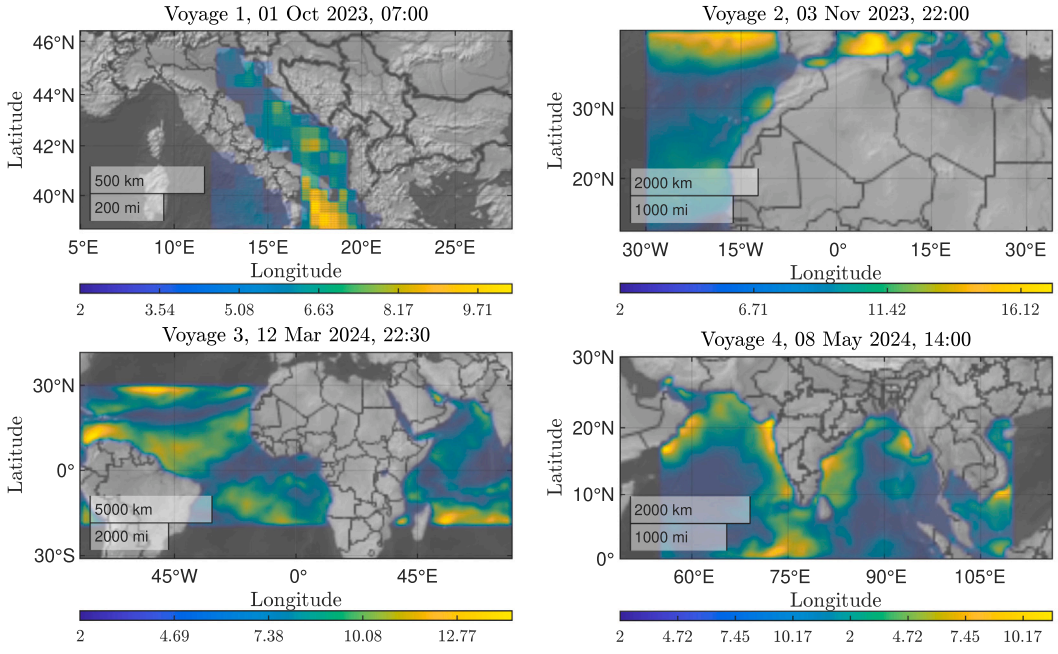

(b) Wind speed $m.s^{-1}$

Fig. 12. Combined significant height of wind and swell waves and wind speed of the considered voyages at the departure time obtained from the ERA5 dataset.

like particle swarm optimization, GWO demonstrates better performance in handling noisy data and is less sensitive to search space variations [68].

GWO is particularly suitable for the ship routing problem due to its ability to handle nonlinear, high-dimensional, and non-convex search spaces with multiple conflicting objectives. Additionally, it requires fewer parameter tuning efforts compared to other swarm-based algorithms.

In the GWO algorithm, the population of candidate solutions is modeled as a pack of wolves. The best solution found so far is considered the alpha (α), followed by the second-best (beta, β), and third-best (delta, δ) solutions. The rest of the population is denoted as omega (ω) wolves. α are the most dominant wolves responsible for decision-making. β wolves are the second in command, assisting the α in decision-making. Subordinate wolves are δ that support α and β in leadership. ω are the lowest-ranking wolves, following the pack's orders. This hierarchical structure is mathematically represented in the optimization algorithm that provides a balance between exploration and exploitation.

The optimization process follows three main stages inspired by grey wolf hunting: tracking, encircling, and attack towards the prey. During each iteration, all wolves update their positions in the search space by following the guidance of the α, β, and δ wolves using mathematically modeled encircling and hunting mechanisms. The interaction between wolves and their prey determines the movement of wolves in the

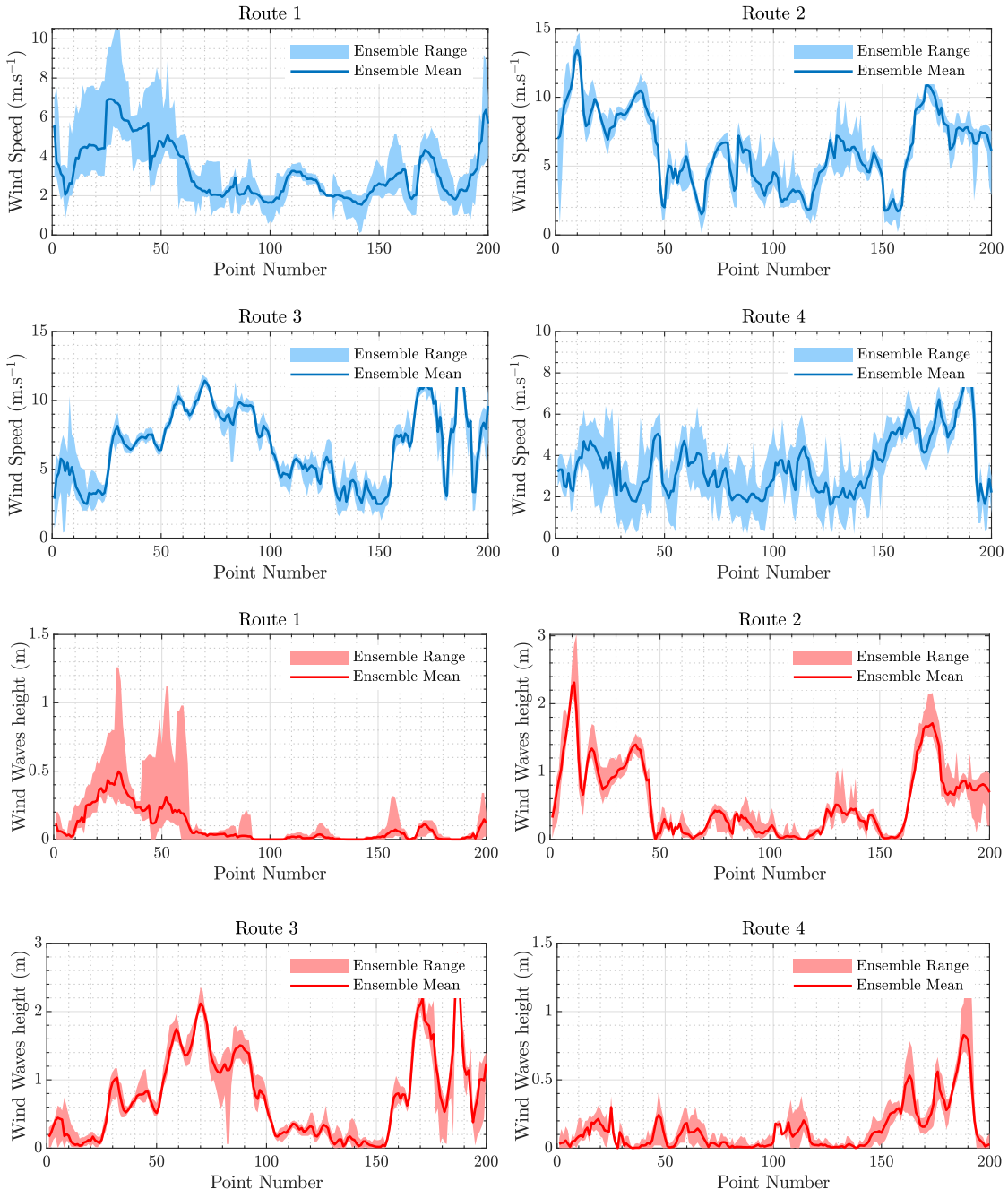

Fig. 13. The collected ensemble wind speed and significant height of wind waves for desired paths of the studied voyages.

optimization process. The distance between a wolf and the prey is given by [9]:

$$\vec{D} = \left|\vec{C} \cdot \vec{X}_p(t) - \vec{X}(t)\right| \tag{21}$$

where t indicates the current iteration, $\vec{X}_p(t)$ represents the prey's position, and $\vec{X}(t)$ denotes the position of a grey wolf in the population. The coefficient vector $\vec{C}$ introduces randomness to simulate unpredictable hunting behavior. The position of a wolf in the next iteration is updated as:

$$\vec{X}(t+1) = \vec{X}_p(t) - \vec{A} \cdot \vec{D} \tag{22}$$

here, $\vec{A}$ modulates the step size and direction of movement toward the prey, contributing to the balance between exploration and exploitation.

The vectors $\vec{A}$ and $\vec{C}$ are defined as:

$$\vec{A} = 2a \cdot \vec{r}_1 - \vec{a} \tag{23}$$

$$\vec{C} = 2 \cdot \vec{r}_2 \tag{24}$$

where $\vec{a}$ decreases linearly over iterations from 2 to 0 to regulate the transition from exploration to exploitation. The random vectors $\vec{r}_1$ and $\vec{r}_2$ are in the range [0,1], which ensures a diverse search pattern.

The position update for each wolf is based on the following equations:

$$\vec{D}_\alpha = |\vec{C}_1 \cdot \vec{X}_\alpha - \vec{X}|, \tag{25}$$

$$\vec{D}_\beta = |\vec{C}_2 \cdot \vec{X}_\beta - \vec{X}|, \tag{26}$$

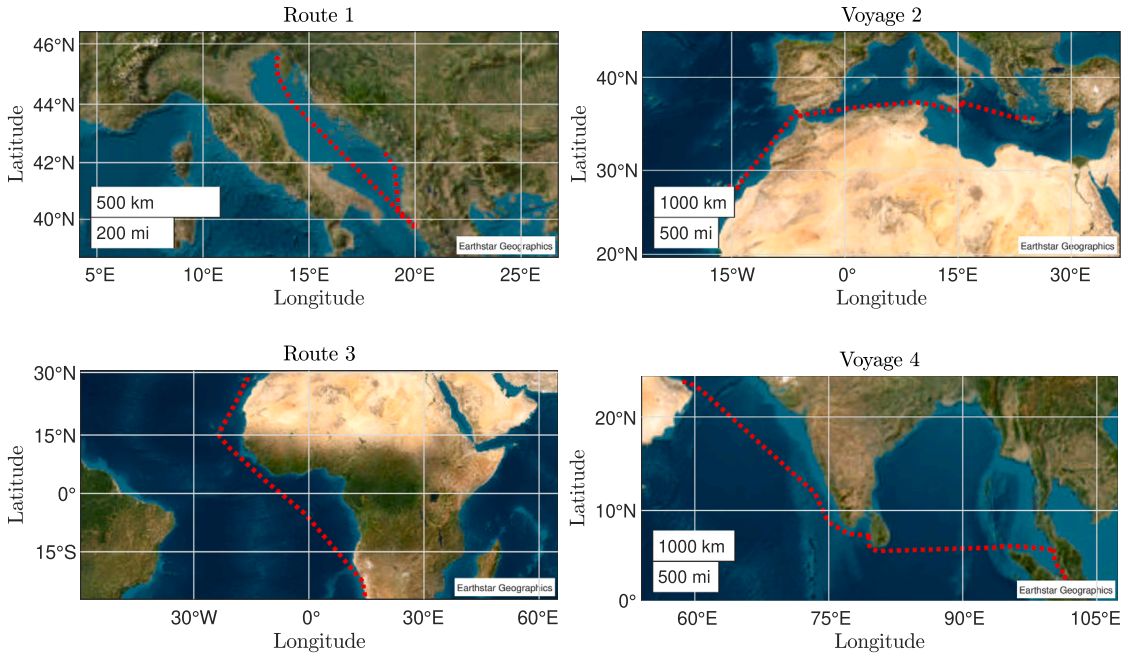

Fig. 14. Geographical maps of the selected paths of the considered voyages to show weather uncertainties.

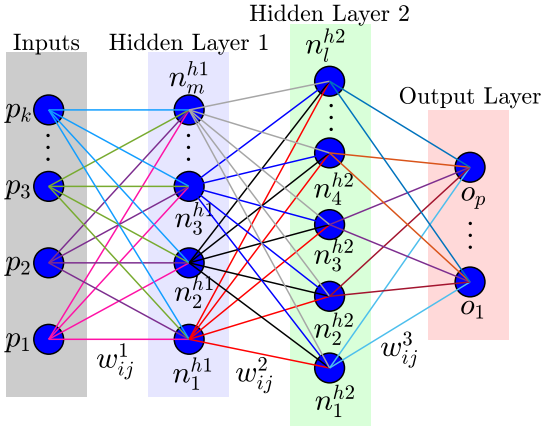

Fig. 15. A schematic diagram of a three-layer MLP neural network.

$$\vec{D}_\delta = |\vec{C}_3 \cdot \vec{X}_\delta - \vec{X}|, \tag{27}$$

$$\vec{X}_1 = \vec{X}_\alpha - \vec{A}_1 \cdot \vec{D}_\alpha, \tag{28}$$

$$\vec{X}_2 = \vec{X}_\beta - \vec{A}_2 \cdot \vec{D}_\beta, \tag{29}$$

$$\vec{X}_3 = \vec{X}_\delta - \vec{A}_3 \cdot \vec{D}_\delta, \tag{30}$$

where $\vec{X}_\alpha$, $\vec{X}_\beta$, and $\vec{X}_\delta$ are the position vectors of the top three wolves, and $\vec{A}_i$, $\vec{C}_i$ are coefficient vectors controlling exploration and exploitation behavior, which change dynamically over iterations. As an example, Fig. 16 shows the mechanism of updating the positions of search agents on a 2D plane. This figure includes a circular search space, a prey at the center, multiple wolf agents positioned around the circle, a wolf to show converging ($|A| < 1$), and diverging ($|A| > 1$). Finally, the new position of the wolf is obtained as the average of these influence points:

$$\vec{X}(t+1) = \frac{1}{3}(\vec{X}_1 + \vec{X}_2 + \vec{X}_3), \tag{31}$$

The GWO relies on two main control parameters: $\vec{A}$ and $\vec{C}$. The vector $\vec{A}$ is linearly decreased over the course of iterations and typically takes random values in the range $[-2a, 2a]$. The magnitude of $\vec{A}$ controls the balance between exploration and exploitation (See Fig. 16). Specifically, when $|\vec{A}| < 1$, the search agents are encouraged to converge towards the best solution found so far, simulating an attack on the prey. In contrast, when $|\vec{A}| > 1$, the agents diverge from the current best solution to explore the search space more broadly in search of better alternatives. This mechanism ensures that the algorithm can alternate between local exploitation and global exploration depending on the value of $\vec{A}$. The second vector, $\vec{C}$, is composed of random values uniformly sampled from the interval $[0, 2]$ and is used to introduce randomness in the distance between the grey wolves and the prey. Unlike $\vec{A}$, the $\vec{C}$ parameter does not decrease over time, thereby maintaining a high degree of randomness throughout the optimization process. This continuous stochastic influence favors global exploration not only during the early iterations but also in the later stages, preventing premature convergence [10]. The pseudocode of the GWO is shown in Algorithm 1.

In the proposed framework, each grey wolf represents a candidate ship route, whose position vector encodes the decision variables of the optimization problem, namely the heading angles and vessel speeds at each route segment. Given a wolf position, the corresponding route waypoints are sequentially generated using the route definition equations, starting from the departure port and advancing segment by segment toward the destination. For each generated route, ensemble-based weather and sea state parameters are assigned to the route segments, and the associated objective functions, including fuel consumption, arrival time deviation, and route smoothness, are evaluated. The multi-objective optimization problem is transformed into a scalar fitness value using a weighted aggregation of the objective functions, where the expected cost over all ensemble members is computed. During each iteration of the GWO, the positions of the wolves are updated based on the guidance of the alpha, beta, and delta solutions, leading to new candidate values of the heading angles and speeds. This iterative process continues until convergence criteria are satisfied, yielding an optimized ship route that balances multiple objectives while satisfying navigational and environmental constraints.

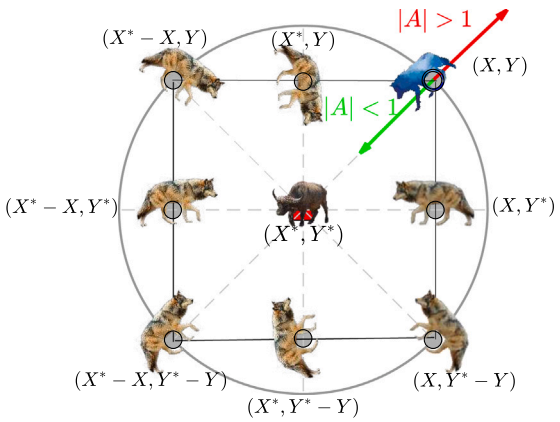

Fig. 16. The mechanism of updating the positions of search agents on a 2D plane and the impact of A on this process.

Algorithm 1 Grey Wolf Optimizer Pseudocode

Input: Objective function $f(\vec{X})$, number of wolves N, maximum iterations T
Output: Best solution $\vec{X}_\alpha$
Initialize the positions of N grey wolves $\vec{X}_i$ $(i = 1, 2, \ldots, N)$ randomly
Evaluate the fitness of each search agent
Identify the best three solutions: $\vec{X}_\alpha$ (best), $\vec{X}_\beta$ (second), $\vec{X}_\delta$ (third)
for $t = 1$ to T **do**
  Update the coefficient a (linearly decreasing from 2 to 0)
  for each search agent i **do**
    for each dimension d **do**
      Generate random vectors $\vec{A}_1$, $\vec{A}_2$, $\vec{A}_3$, and $\vec{C}_1$, $\vec{C}_2$, $\vec{C}_3$
      Compute:

$$\vec{D}_\alpha = |\vec{C}_1 \cdot \vec{X}_\alpha - \vec{X}_i|,$$
$$\vec{D}_\beta = |\vec{C}_2 \cdot \vec{X}_\beta - \vec{X}_i|,$$
$$\vec{D}_\delta = |\vec{C}_3 \cdot \vec{X}_\delta - \vec{X}_i|$$
$$\vec{X}_1 = \vec{X}_\alpha - \vec{A}_1 \cdot \vec{D}_\alpha$$
$$\vec{X}_2 = \vec{X}_\beta - \vec{A}_2 \cdot \vec{D}_\beta$$
$$\vec{X}_3 = \vec{X}_\delta - \vec{A}_3 \cdot \vec{D}_\delta$$

      Update position:

$$\vec{X}_i^{(t+1)} = \frac{1}{3}(\vec{X}_1 + \vec{X}_2 + \vec{X}_3)$$

    end for
  end for
  Evaluate new positions of search agents
  Update $\vec{X}_\alpha$, $\vec{X}_\beta$, $\vec{X}_\delta$
end for
return $\vec{X}_\alpha$ as the best solution found

The application of the GWO algorithm to the weather routing problem proceeds as follows:

1. **Initialization:** Generate an initial population of N search agents (wolves), where each agent represents a candidate route vector $\vec{X}_i = [\theta_1, v_1, \ldots, \theta_K, v_K]$ containing heading angles and speeds for all K waypoints.
2. **Fitness Evaluation:** Evaluate the fitness of each agent using the combined objective function J (Eq. (12)). This involves simulating the voyage for each route $\vec{X}_i$ to calculate the fuel consumption (J_{fuel}), arrival time deviation (J_{time}), and smoothness (J_{smooth}).
3. **Hierarchy Update:** Sort the population based on fitness values. The three agents with the lowest J values are designated as the leaders: α (best), β (second best), and δ (third best).
4. **Parameter Tuning:** Update the convergence factor $\vec{a}$, which decreases linearly from 2 to 0 over the course of iterations. This tuning parameter controls the coefficient vectors $\vec{A}$ and $\vec{C}$, shifting the search behavior from global exploration (early iterations) to local exploitation (later iterations).
5. **Position Update:** Update the position of the remaining ω wolves based on the distance vectors to the leaders $\alpha, \beta,$ and δ. The new heading and speed variables are adjusted to converge towards the optimal regions of the search space.
6. **Termination:** Repeat steps 2–5 until the maximum number of iterations is reached, returning $\vec{X}_\alpha$ as the optimal route solution.

7. Results and discussion

7.1. Developing the ship fuel consumption prediction model

The predictive model for ship fuel consumption is developed using an MLP neural network model with Bayesian Hyperparameter Optimization. Bayesian optimization is a process aimed at minimizing an objective function, which in this study is the MSE of the model predictions. This process involves iteratively selecting hyperparameter values that improve the model's performance. The model is trained using input parameters that include AT, AH, SST, RWS, RWD, SHTS, MPTS, MDTS, SHWW, MPWW, MDWW, and STW. The output of the model is the MFC. The MLP neural network setup is designed with optimizable hyperparameters which allow for an adaptive architecture. The number of fully connected layers is searched among configurations with 1, 2, and 3 layers. The size of each layer is log-scaled and searched within the range of integers [1, 300]. The activation function is selected from four options: ReLU, Tanh, None, and Sigmoid. Regularization strength, denoted as Lambda, is searched among real values log-scaled within the range $[0.00001/n, 100000/n]$, where n represents the number of observations in the dataset. Data standardization is enabled to ensure uniformity in input scales, and a 5-fold cross-validation strategy is employed to enhance model robustness. To evaluate the model's performance during the training process, 15% of the total dataset is reserved for testing. This set is essential for verifying the model's ability to generalize and perform well on new, unseen data. Bayesian optimization is configured with an acquisition function known as Expected Improvement Per Second Plus [62], which balances exploration and exploitation by targeting hyperparameter combinations with the potential to improve the objective function efficiently. The optimization process is set to iterate 30 times, with each iteration corresponding to a distinct combination of hyperparameter values tested during model training.

The final optimized neural network consists of two fully connected layers, with the first layer containing 26 neurons and the second layer 3 neurons. The network uses the Tanh activation function, which introduces non-linearity and allows the network to learn complex patterns. Regularization is applied with a Lambda of 0.00167, helping to prevent overfitting by penalizing large weights. Fig. 17 shows the minimum Mean Square Error (MSE) vs. iterations plot of the final generated optimized neural network model. The MAE of 0.5538 (kg min^{-1}) and the RMSE of 1.0391 (kg min^{-1}) indicate that the model's predictions are close to the actual values, showcasing its accuracy. With a Mean Absolute Percentage Error (MAPE) of 0.8575%, the model demonstrates a suitable ability to predict fuel consumption with minimal relative error. Finally, the R-squared (R^2) value of 0.9972 signifies an acceptable fit. The ANN predicted vs. actual value of the training data is shown in Fig. 18. Additionally, the prediction error histogram is presented in this figure.

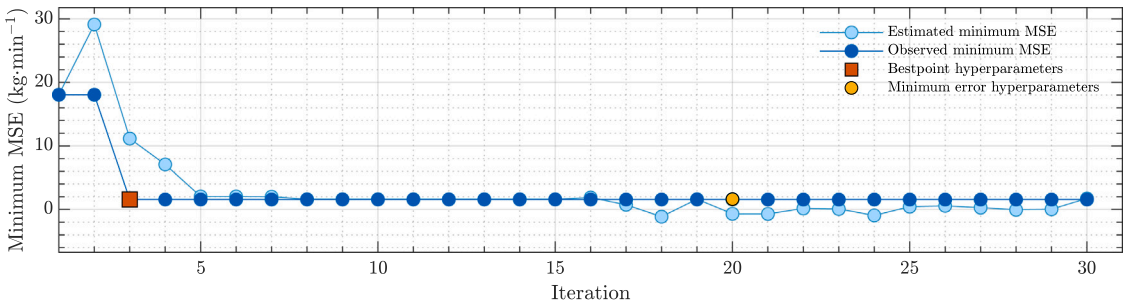

Fig. 17. The minimum MSE vs. iterations plot of the generated optimized neural network model based on training data for the total ship fuel consumption prediction.

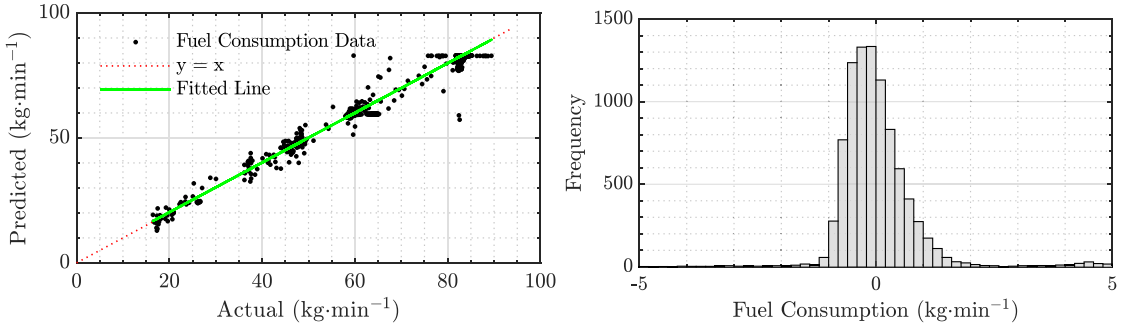

(a) The actual vs. predicted values. (b) Prediction error histogram

Fig. 18. The generated optimized neural network model based on training data for the total ship fuel consumption prediction.

7.2. Optimization setup and assumptions

To evaluate the performance of the proposed ensemble-based multi-objective weather routing framework, the optimization model is configured using realistic operational and environmental assumptions derived from real-world voyage scenarios. The framework is applied to four case study routes of varying length and complexity, connecting ports across Europe, Africa, and Asia, as outlined in Table 2.

The following assumptions are made in this study: Ship maneuverability is limited by a maximum heading angle change constraint of $\Delta\theta_{\max} = 30°$ per segment [33], except when encountering obstacles. Ship speed is constrained within the range $v_k \in [5, 20]$ knots to reflect practical limits. To reflect realistic ship maneuvering behavior in port areas, it is assumed that the vessel starts its voyage with a low initial speed and gradually accelerates to its cruising speed within the first route segment. Similarly, during the final segment, the vessel decelerates smoothly in preparation for docking. Therefore, the speed at the initial and final segments is constrained to be within a reduced operational range, typically between 6 and 10 knots. For simplicity and model consistency, it is assumed that the vessel maintains a constant speed over each route segment, including the first and last. Significant wave heights and wind speeds must remain below $H_s \leq 6$ m and $W_s \leq 20$ m s^{-1} for safe operation (aligning with IMO guidelines for adverse weather avoidance [69]). The bathymetric constraint is defined based on the draught of the case study vessel, which draws approximately 8 m. A 20% safety margin [70] is applied, requiring all route points to lie within cells with water depths of at least 9.6 m.

The number of search agents (wolves) is set to $N = 100$, and the maximum number of iterations is set to $T = 300$. The parameters controlling the exploration–exploitation balance are initialized as $a = 2$ (linearly decreasing to 0), while the random coefficient vector $\vec{C}$ is sampled uniformly from $[0, 2]$ in each iteration. Moreover, as mentioned, the Bootstrapping method is used to ensure all variables have an equal number of ensemble members by resampling with replacement from available data. The number of weather parameters ensemble members M is set to 50.

7.3. Effect of ensemble contributions on optimization performance

In all studied objectives (Section 3.5), the weights of fuel, ETA deviation, and route smoothness are initially chosen as $w_1 = 0.5$, $w_2 = 0.4$, and $w_3 = 0.1$, respectively, to prioritize fuel efficiency while maintaining timeliness and maneuverability.

7.3.1. Mean strategy results

In this study, the mean strategy is primarily adopted to account for the variability of environmental conditions, promoting solutions that are robust on average across multiple weather ensemble realizations. Fig. 19 depicts the initial route population generation (search agents) for the considered voyages. Each route is composed of multiple segments, and for each segment, the heading angle and ship speed are randomly assigned within predefined physical and operational bounds. The number of segments may vary across routes, allowing diverse initial connectivity patterns between the departure and destination points. This stochastic initialization ensures broad exploration of the search space and provides a diverse starting point for the GWO algorithm. This figure illustrates the total voyage duration, distance traveled, and estimated fuel consumption for each initial route.

The geographical maps of the obtained optimal voyages by the ensemble mean strategy are shown in Fig. 20. It illustrates optimized routes that minimize the average cost across all members of the ensemble. These routes represent the best trade-offs between travel time, distance, and fuel consumption, considering the ensemble-averaged of the cost function across all ensemble members. The results demonstrate the algorithm's ability to adapt the routing decisions to the spatial variability in marine weather and provide efficient passage planning. Moreover, to assess the computational effectiveness of the proposed optimization framework, the convergence history of the GWO algorithm is analyzed. Fig. 21 illustrates the minimization of the combined weighted objective function over 300 iterations for the four case study voyages. The results indicate a sharp reduction in the objective value within the initial iterations, demonstrating the algorithm's acceptable

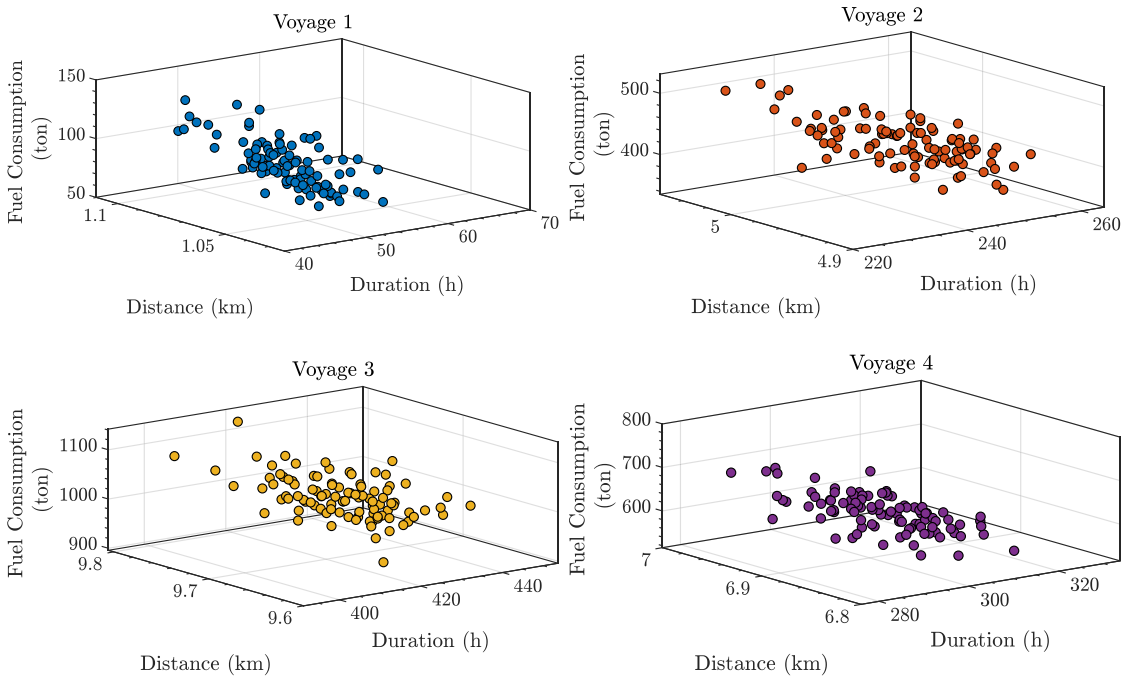

Fig. 19. Initial route population generation (search agents) for the optimization purpose of the considered voyages.

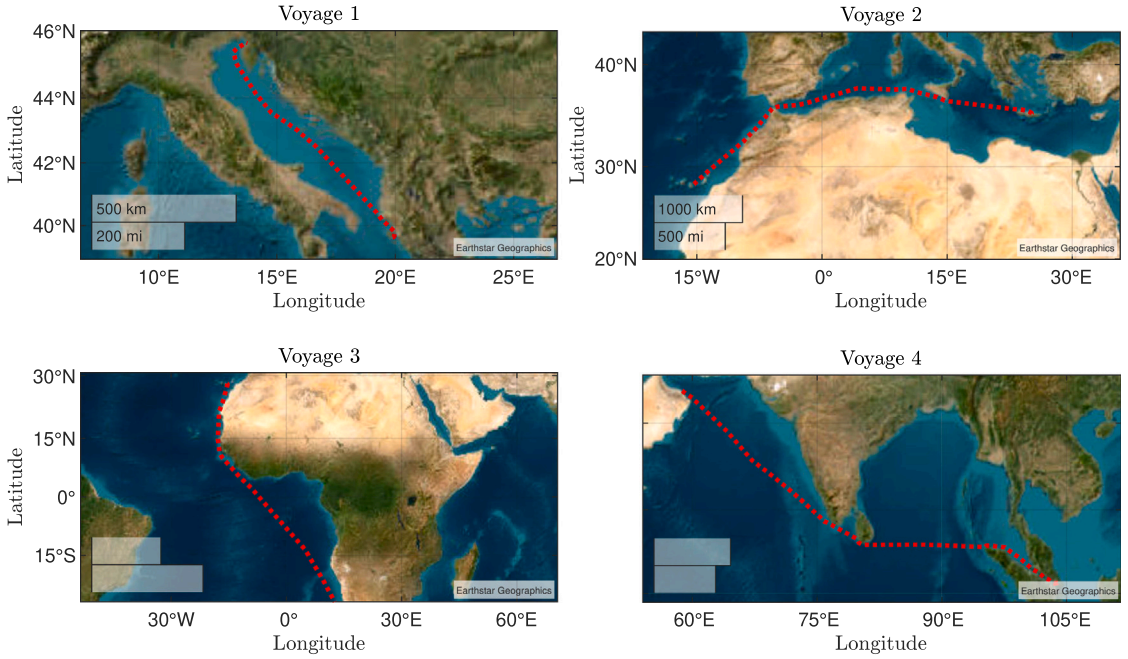

Fig. 20. Geographical maps of the obtained optimal voyages by the ensemble mean strategy.

exploration capabilities. Subsequently, the curve stabilizes, reflecting the exploitation phase where the GWO refines the solution locally. Fig. 22 presents different timestamps along the obtained optimal voyage 4. The background shading represents the ensemble-averaged combined significant wave height of wind and swell waves at each corresponding time. This visualization highlights how the route dynamically interacts with evolving sea state conditions throughout the voyage.

Fig. 23 presents 3D scatter plots of leg-wise distance, duration, and speed over ground for the four optimized voyages obtained using the ensemble mean strategy. Each subplot illustrates how the vessel's speed and travel time vary across segments along the total voyage distance. The statistical analysis of the optimized voyage legs reveals distinct routing behaviors among the four case studies, highlighting variations in speed, distance, and duration. Voyage 1 shows high variability in leg distances and a stable speed profile, whereas Voyage 2 maintains higher speeds over longer distances but exhibits diverse transit times. Voyage 3 has the lowest speeds, while Voyage 4 features the slowest average speed with relatively uniform transit times, reflecting strategic fuel management and time of arrival.

The fuel consumption and propeller RPM box plot of the generated legs are shown in Fig. 24. The analysis of the optimized voyage legs reveals notable variations in fuel consumption and propeller RPM across the four case studies. Voyage 1 exhibited a highly skewed fuel profile with a mean of 2164.3 kg. In contrast, Voyage 3 showed more

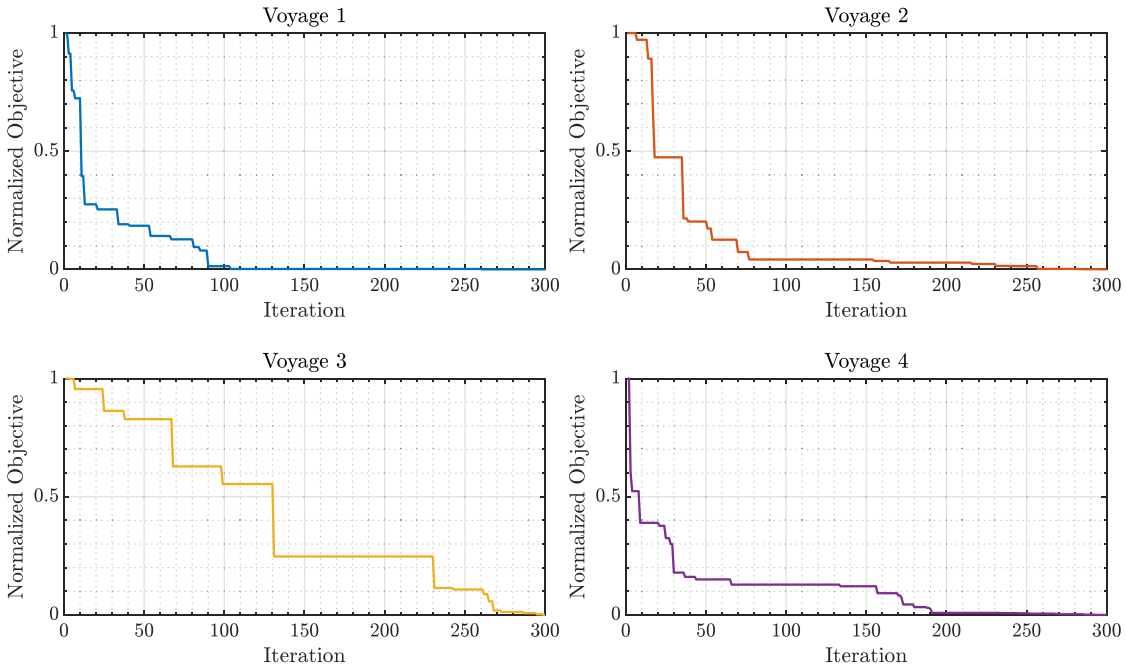

Fig. 21. Convergence curve of the obtained optimal voyages by the ensemble mean strategy.

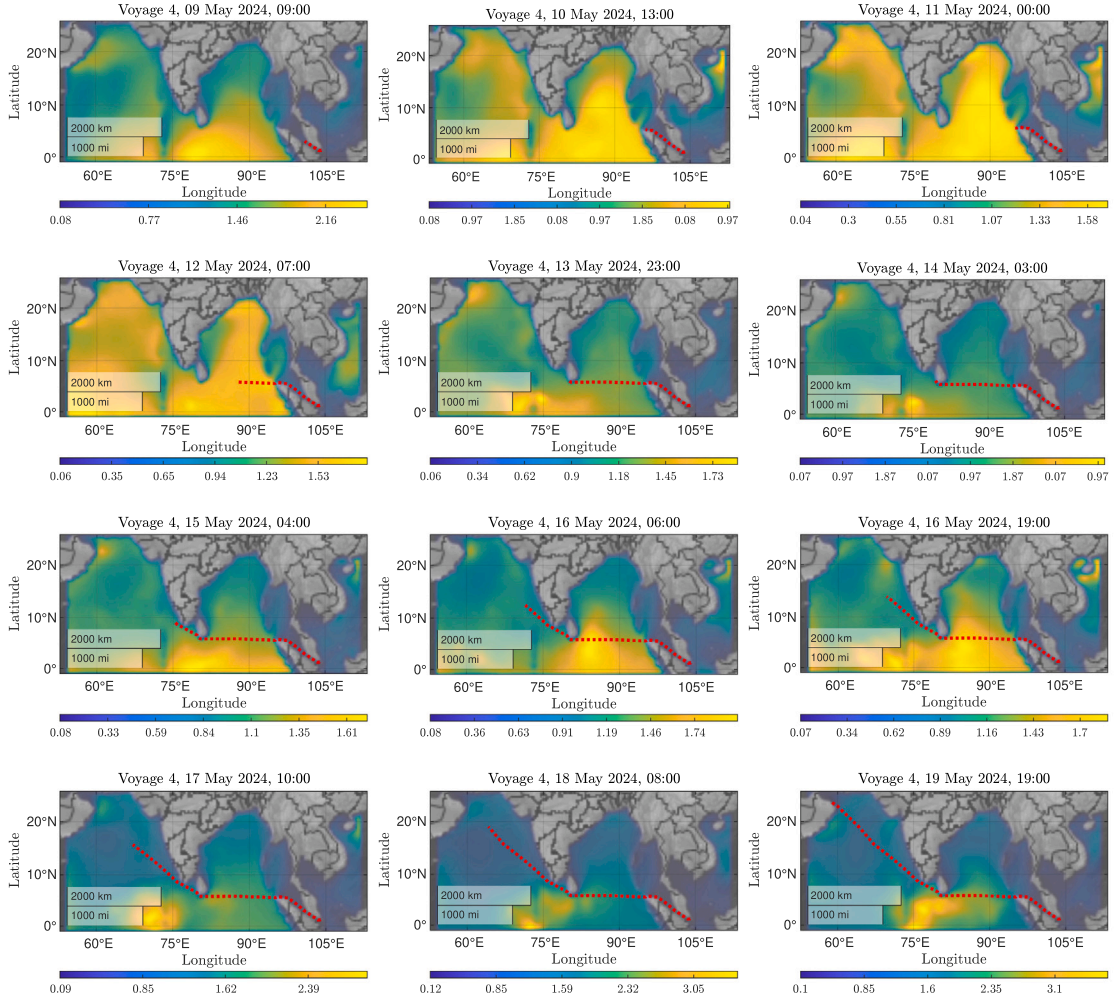

Fig. 22. Different timestamps of the obtained optimal voyage 4 by the ensemble mean strategy with the ensemble mean of the combined significant height of wind and swell waves.

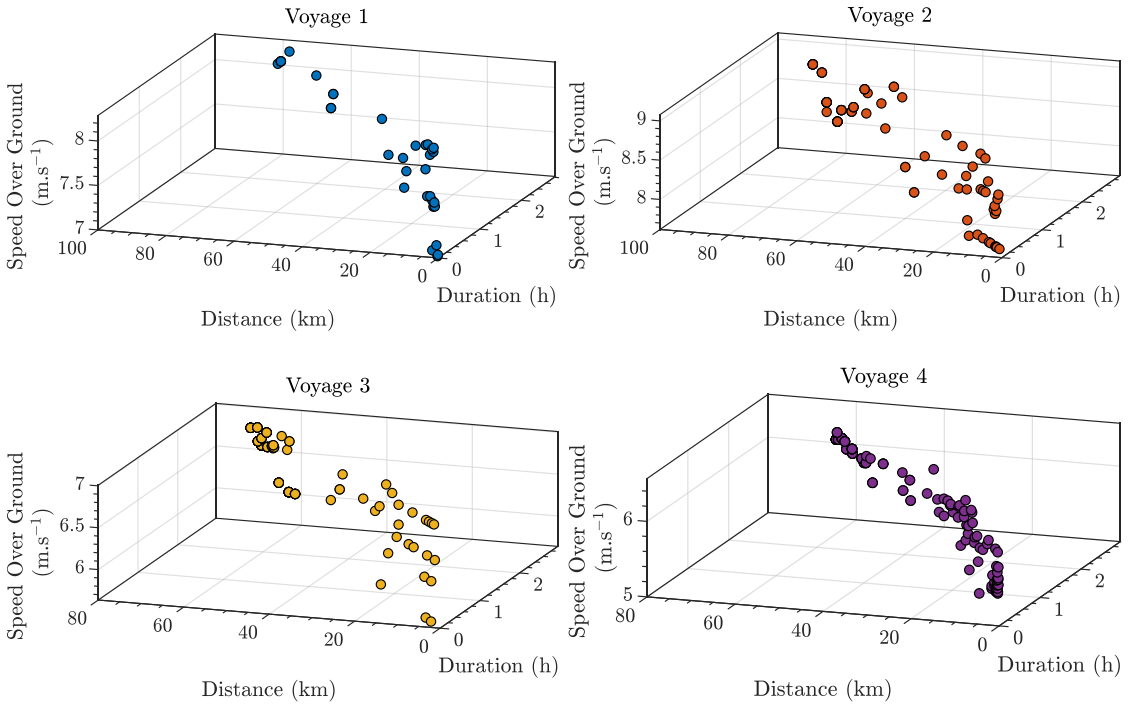

Fig. 23. Generated leg details of the obtained optimal voyages by the ensemble mean strategy.

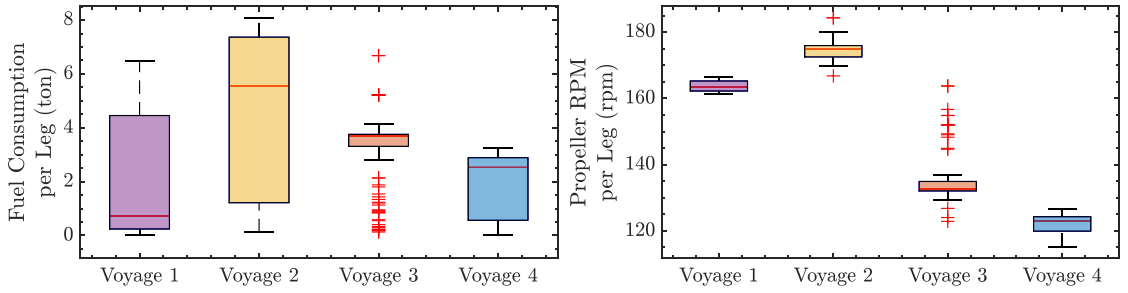

Fig. 24. The fuel consumption and propeller RPM box plot of the generated leg details of the obtained optimal voyages by the ensemble mean strategy.

uniform fuel use among legs, with a mean of 3269.6 kg and tighter interquartile range (Q1 = 3307.5 kg, Q3 = 3754.6 kg), suggesting consistent energy demand. Regarding propeller performance, Voyage 1 maintained a nearly constant RPM (mean = 164.39, std = 0.02), indicating steady cruising conditions. However, Voyage 3 demonstrated the highest variability in RPM (std = 6.95), reflecting more frequent speed adjustments or changing sea states.

Fig. 25 shows the fuel consumption over time across the obtained optimal voyages. 200 waypoints are selected across the obtained optimal routes. The shaded region represents the ensemble mean ± standard deviation. The differences in the width of the shaded regions suggest varying degrees of uncertainty in fuel consumption across different voyages. Moreover, Table 5 summarizes the performance characteristics of the four optimized voyages. Distance, Time, and Fuel refer to the total traveled distance, total traveled time, and total fuel consumed per voyage, respectively, while speed represents the average speed over ground. RPM indicates the average propeller rotation per minute. The voyage distances range from approximately 924 km (Voyage 1) to 8246 km (Voyage 3), with corresponding durations from 32 h up to 351.6 h. The highest average speed was observed in Voyage 2 (8.384 m s^{-1}), which also recorded the highest average propeller RPM (173.948 rpm), indicating a relatively faster transit. In contrast, Voyage 4 exhibited the lowest speed (6.047 m s^{-1}) and RPM (123.244 rpm), suggesting more fuel-efficient but slower navigation. Despite being the longest in distance and duration, Voyage 3 consumed the most fuel (474,097 kg), while the shortest Voyage 1 required the least (73,587 kg). Moreover, the optimized voyages demonstrate acceptable alignment with the scheduled arrival times. Voyage 1 arrived 10 min early, Voyage 2 arrived 19 min early, and Voyage 3 arrived 26 min ahead of schedule—indicating precise control over voyage timing. Voyage 4 arrived 21 min earlier than planned, which is a minor deviation over a long-duration journey. Overall, the optimization maintains acceptable accuracy in arrival scheduling across all four voyages.

The normalized performance indicators for the four optimal voyages are shown in Fig. 26, which reveals distinct trade-offs between fuel consumption per kilometer, CO_2 emissions per kilometer, speed, and voyage duration. Voyage 1 demonstrates balanced performance, achieving high operational efficiency with relatively low fuel and emission intensities, high speed, and the shortest duration. Voyage 2, while achieving the highest speed and relatively short duration, exhibits the highest fuel and CO_2 intensities, indicating a trade-off favoring time over environmental impact. In contrast, Voyage 3 stands out for its minimum fuel and emission rates per kilometer, making it the most environmentally efficient, albeit with a significant penalty in speed and duration. Voyage 4, with the lowest scores in almost all criteria except voyage duration, indicates the least favorable performance overall. Notably, these performance variations are not solely attributed to the routing strategy but are also significantly influenced by the prevailing

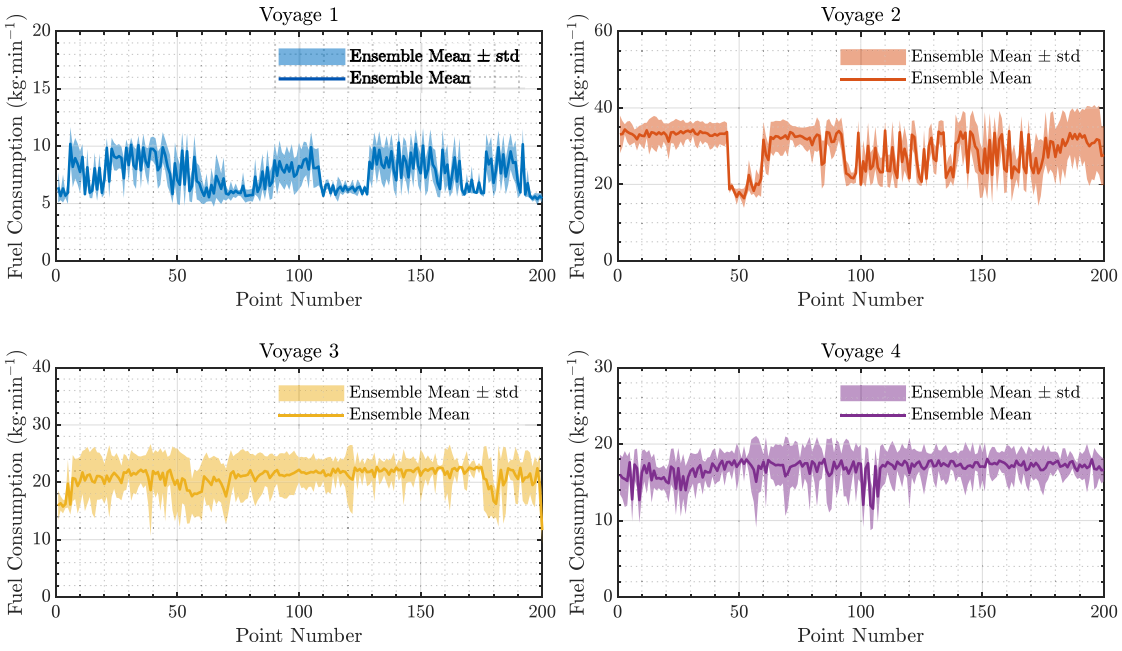

Fig. 25. Fuel consumption uncertainty over time across the obtained optimal voyages by the ensemble mean strategy.

Table 5
The obtained optimal voyage statistics by the ensemble mean strategy.

Voyage	Distance (km)	Time (h)	Speed (m s^{-1})	RPM (rpm)	Fuel (kg)	Arrival
1	924.517	31.833	8.025	164.382	73 577.355	2023-10-02T14:49:57Z
2	4085.774	135.362	8.384	173.948	371 944.621	2023-11-09T13:11:41Z
3	8245.989	351.567	6.515	134.486	474 078.314	2024-03-27T14:04:00Z
4	5863.839	269.369	6.047	123.244	275 714.883	2024-05-19T19:09:07Z

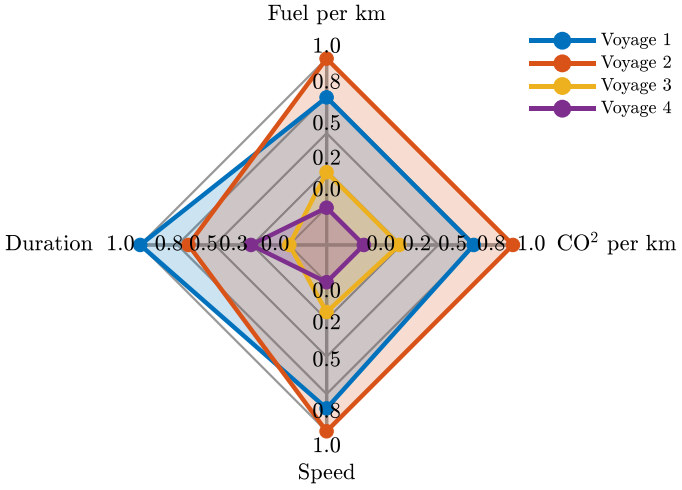

Fig. 26. Normalized performance comparison across the obtained optimal voyages by the ensemble mean strategy.

weather conditions along each route. Environmental parameters such as wind, waves, and currents substantially affect both energy efficiency and sailing time, underscoring the necessity to integrate weather uncertainties into performance evaluations and comparative analyses.

To assess the robustness of the proposed ensemble-based Grey Wolf Optimizer under stochastic variability, each case study voyage is optimized using 30 independent runs with different random initial populations. Table 6 reports the mean and standard deviation of key voyage performance indicators. The reported mean values differ from the deterministic single-run results due to the stochastic exploration of the solution space, while remaining within physically reasonable bounds. The relatively low standard deviations observed for distance, travel time, fuel consumption, and operational speed indicate consistent convergence behavior across repeated runs. Moreover, the arrival time deviation remains limited for all voyages, confirming the ability of the optimization framework to reliably satisfy just-in-time arrival constraints. These results demonstrate that, despite its stochastic nature, the proposed GWO-based framework produces stable, repeatable, and operationally feasible routing solutions under ensemble weather uncertainty.

Table 6
Statistical performance of the proposed framework over 30 independent runs using the ensemble mean strategy (Mean ± Std).

Voyage	Distance (km)	Time (h)	Speed (m s^{-1})	RPM (rpm)	Fuel (kg)	Arrival deviation (h)
1	932.8 ± 21.6	32.4 ± 1.2	7.91 ± 0.28	162.1 ± 6.3	$7.51 \times 10^4 \pm 2.4 \times 10^3$	0.48 ± 0.21
2	4152.3 ± 79.5	138.9 ± 3.8	8.17 ± 0.26	171.4 ± 7.2	$3.86 \times 10^5 \pm 1.1 \times 10^4$	0.74 ± 0.29
3	8391.6 ± 142.8	358.7 ± 7.6	6.31 ± 0.22	131.2 ± 5.6	$4.92 \times 10^5 \pm 1.6 \times 10^4$	1.03 ± 0.41
4	6024.7 ± 118.9	275.6 ± 6.3	5.84 ± 0.19	120.5 ± 4.8	$2.89 \times 10^5 \pm 9.1 \times 10^3$	0.66 ± 0.27

Table 7
The obtained optimal voyage statistics by the worst-case strategy.

Voyage	Distance (km)	Time (h)	Speed (m s^{-1})	RPM (rpm)	Fuel (kg)	Arrival
1	975.526	31.852	9.031	185.245	82 221.015	2023-10-02T14:51:07Z
2	4111.256	135.372	9.154	187.154	395 068.371	2023-11-09T13:22:19Z
3	8310.625	351.779	7.925	164.017	505 307.878	2024-03-27T14:16:14Z
4	5935.841	269.415	7.417	159.741	287 736.004	2024-05-19T19:24:55Z

7.3.2. Worst-case strategy results

The worst-case optimization approach is employed to ensure robustness against adverse weather conditions. In this approach, the voyage cost is evaluated across all ensemble members representing possible weather realizations. Instead of minimizing the mean value, the optimization aims to minimize the maximum cost among all ensemble members. The resulting routes are thus more conservative but provide higher reliability, especially in critical operational contexts. Table 7 presents the results of the optimal voyages obtained using the worst-case strategy. Compared to the mean strategy, the voyages under the worst-case formulation exhibit increased total distances and fuel consumption, indicating that the optimizer selected more robust routes to mitigate the impact of adverse weather conditions. The ship speeds and engine RPMs are also higher across all voyages to ensure timely arrivals despite challenging scenarios.

7.3.3. Risk-aware (mean–variance) approach results

In addition to the mean value and worst-case strategies, a risk-aware optimization approach is considered by formulating the objective function based on the mean–variance criterion. This method simultaneously minimizes the expected fuel consumption while penalizing high variability among the ensemble members, thereby achieving a balance between performance efficiency and operational reliability. By incorporating variance into the objective function, the optimizer aims to select routes and operating conditions that are not only fuel-efficient on average but also less sensitive to uncertain and fluctuating weather conditions. This approach provides a practical middle ground between the optimistic (mean-based) and conservative (worst-case) strategies. The results obtained from this strategy are discussed and compared in the following. A reasonable starting point for selecting the value of λ in the risk-aware cost function (Eq. (19)) depends on the relative scale of the expected cost $\mathbb{E}[J]$ and its standard deviation std(J). A guidance method to select a suitable value for λ is to plot the Pareto front of mean vs. std for different λ values to visually select the most suitable trade-off for the considered application. Here, $\lambda = 1$ is considered, which gives equal weight to the mean and standard deviation. This provides a balanced trade-off between fuel efficiency and robustness.

Table 8 presents the obtained optimal voyage statistics using the Risk-aware strategy. Compared to the mean strategy (Table 5), this approach results in slightly longer traveled distances and marginally increased fuel consumption for all voyages. This trade-off is a result of incorporating the variability (standard deviation) of the ensemble-based cost, which leads the optimizer to prefer more stable and less uncertain routes. In contrast to the worst-case strategy (Table 7), the Risk-aware approach achieves lower fuel consumption and avoids the overly conservative behavior that characterizes the worst-case design. The voyage times remain nearly identical across all strategies, ensuring compliance with the predefined arrival schedule. Overall, the Risk-aware strategy provides a balanced solution that enhances robustness against weather uncertainties while maintaining operational efficiency and minimizing unnecessary fuel penalties.

7.3.4. Conditional value-at-risk approach results

In this subsection, the optimal voyage planning results are evaluated using the CVaR strategy, which aims to control the mean cost in the worst α-tail of the distribution. The CVaR approach offers a compromise between the conservative nature of the worst-case strategy and the average-based strategies. The α value is set to 0.95, which means the optimization targets the mean of the worst 5% scenarios across the ensemble simulations. Table 9 presents the final simulation results obtained using the CVaR strategy with a confidence level of $\alpha = 95\%$. As observed, the CVaR-based routing decisions result in increased fuel consumption compared to the ensemble mean strategy, particularly due to the selection of more conservative speeds and RPM values. However, they offer substantial savings compared to the worst-case strategy, thereby achieving a trade-off between performance and robustness. Furthermore, the arrival times across all voyages remain within the acceptable limits of the planned schedule, confirming the feasibility of the CVaR-based approach in maintaining punctuality while accounting for uncertainty.

7.4. Discussion

The results presented in Tables 5–9 provide a comprehensive comparative analysis of four different objective function strategies for ensemble-based ship routing optimization. Each strategy exhibits distinct characteristics that show different trade-offs between fuel efficiency, voyage robustness, and adherence to arrival time constraints under uncertain weather conditions.

The ensemble mean strategy (Table 5) prioritizes fuel efficiency by optimizing the mean outcome over all ensemble members. This approach resulted in the lowest fuel consumption across most voyages. However, this gain comes at the potential expense of robustness, as the mean strategy may under-prepare the vessel for rare but severe weather scenarios. For instance, the average speeds and RPMs are consistently lower across voyages, which implies a conservative engine setting that may not sufficiently account for adverse weather conditions in the tail of the distribution.

The worst-case strategy (Table 7), by contrast, adopts a highly conservative approach that provides feasibility under the most adverse ensemble scenario. This leads to higher average speeds and engine RPMs across the voyages. For example, Voyage 1 under the worst-case strategy had a speed of 9.031 m s^{-1} and fuel consumption of 82 221.015 kg, both higher than the ensemble mean's 8.025 m s^{-1} and 73 577.355 kg for the same voyage. The slightly longer distances observed in some worst-case voyages (e.g., Voyage 1: 975.526 km vs. 924.517 km for the ensemble mean) further contribute to this increased fuel consumption. Consequently, fuel consumption is significantly higher compared to the other methods. While this strategy maximizes safety, it incurs a substantial fuel penalty, highlighting

Table 8
The obtained optimal voyage statistics by the Risk-aware strategy with $\lambda = 1$.

Voyage	Distance (km)	Time (h)	Speed (m s^{-1})	RPM (rpm)	Fuel (kg)	Arrival
1	960.214	31.921	8.74	173.804	76 233.145	2023-10-02T14:55:14Z
2	4180.851	135.431	8.854	180.254	380 651.796	2023-11-09T13:25:51Z
3	8330.654	351.676	7.02	144.546	485 639.981	2024-03-27T14:10:33Z
4	5912.357	269.321	6.952	142.116	280 451.749	2024-05-19T19:19:17Z

Table 9
The obtained optimal voyage statistics by the CVaR strategy with $\alpha = 95\%$.

Voyage	Distance (km)	Time (h)	Speed (m s^{-1})	RPM (rpm)	Fuel (kg)	Arrival
1	950.121	31.871	8.67	174.724	76 357.885	2023-10-02T14:52:15Z
2	4107.734	135.351	8.72	180.071	382 211.351	2023-11-09T13:21:02Z
3	8400.314	351.745	7.52	156.823	490 475.522	2024-03-27T14:14:43Z
4	5900.738	269.372	7.32	148.504	282 432.178	2024-05-19T19:22:18Z

the inefficiency of overly conservative routing when the worst-case conditions may not materialize in practice.

The risk-aware strategy (Table 8) introduces a tunable risk aversion parameter ($\lambda = 1$ in this case). The results show moderate fuel consumption levels, lying between those of the worst-case and ensemble mean strategies. For example, in Voyage 2, the fuel usage is 380,651 kg, which is higher than the mean strategy (371,944 kg) but lower than the worst-case (395,068 kg). The risk-aware approach also results in slightly more conservative arrival times. This demonstrates its potential for practical applications where operational risks must be mitigated without excessive conservatism.

The CVaR strategy (Table 9) with a confidence level of $\alpha = 95\%$ further refines the risk-aware concept by explicitly focusing on the tail-end risks of the fuel consumption distribution. Its results closely align with those of the risk-aware method, reflecting a well-calibrated trade-off. For example, in Voyage 3, the CVaR strategy achieved a fuel consumption of 490,475 kg, which is lower than the worst-case but higher than the mean. The arrival times and speeds indicate a cautious yet not overly conservative routing profile. This approach is particularly advantageous for ship operators seeking to balance fuel efficiency with risk exposure under uncertainty, as it explicitly accounts for potential extreme outcomes while avoiding the inefficiencies of the worst-case strategy.

Overall, the findings underscore the importance of selecting an appropriate routing strategy based on the specific risk preferences and operational priorities of the voyage. While the ensemble mean strategy is appealing for fuel minimization under average conditions, it may compromise robustness in extreme weather. The worst-case strategy ensures maximum safety but at a significant fuel cost. The risk-aware and CVaR strategies offer a sensible compromise, effectively balancing fuel efficiency with robustness against uncertainty. The optimal choice largely depends on specific operational requirements, environmental conditions, and predefined objectives.

8. Conclusion

This study proposed a novel ensemble-based framework for ship weather routing optimization that addresses the inherent uncertainties in marine weather conditions by incorporating forecasting data directly into the route optimization process. The proposed framework integrated multiple components, including a neural network-based ship performance model developed using onboard data, a Bayesian hyperparameter optimization scheme for model tuning, comprehensive weather data using ensemble forecasts, and a GWO for solving the multi-objective optimization problem. The multi-objective formulation considered key operational targets, including fuel consumption, voyage time and distance, ship speed and heading angle profiles, thereby capturing the trade-offs between efficiency, safety, and operational constraints in realistic scenarios.

Four distinct strategies for handling ensemble weather uncertainties were evaluated: the ensemble mean approach, the worst-case strategy, a risk-aware formulation with a linear risk aversion parameter, and a Conditional Value-at-Risk method at a 95% confidence level. The obtained results highlighted that the objective optimization strategy significantly influences the operational performance of the voyage, especially over longer routes and under variable weather conditions. Specifically, the ensemble mean strategy, while yielding lower fuel consumption in shorter voyages, demonstrated higher sensitivity to weather extremes in longer voyages, potentially compromising safety margins. Conversely, the worst-case strategy, while providing the most conservative route planning, resulted in substantially higher fuel usage and engine loads, underscoring the trade-off between robustness and efficiency.

The risk-aware and CVaR strategies emerged as effective compromises, providing balanced solutions that mitigate excessive fuel usage while maintaining reasonable operational safety against adverse weather conditions. For instance, the CVaR strategy effectively limited exposure to high-risk weather scenarios, resulting in only a marginal increase in fuel consumption compared to the ensemble mean strategy, but with improved reliability and operational stability. The results further emphasized that multi-objective optimization, when combined with an ensemble-based weather uncertainty modeling approach, enables a fine understanding of trade-offs and supports informed decision-making in ship routing operations.

While the proposed ensemble-based framework demonstrates acceptable performance in handling weather uncertainties, several limitations warrant attention in future research to further enhance operational applicability.

- **Pareto-based Optimization:** The current methodology relies on a weighted sum approach to aggregate conflicting objectives (fuel, time, smoothness). While computationally efficient, this requires the a priori determination of weights, which may introduce subjective bias. Future studies should explore Pareto-based algorithms, such as Multi-Objective Grey Wolf Optimizer (MOGWO) or NSGA-III, to generate a comprehensive set of non-dominated solutions. This would allow ship operators to visualize the Pareto front and select the optimal trade-off between fuel efficiency and risk dynamically.
- **Dynamic Seakeeping Constraints:** The present safety constraints utilize static thresholds for significant wave height and wind speed. However, these do not fully capture the complex ship responses to sea states. Future work aims to integrate dynamic seakeeping analyses directly into the cost function, explicitly calculating the probability of dangerous phenomena such as parametric rolling or excessive acceleration based on the ship's specific hull geometry and loading condition.
- **Computational Efficiency:** The evaluation of robust cost functions (e.g., CVaR) across large ensemble datasets is computationally intensive. Investigating the use of surrogate models or

deep reinforcement learning agents to approximate the objective function could significantly reduce calculation times, making the system more viable for real-time onboard implementation.

CRediT authorship contribution statement

Kumars Mahmoodi: Writing – review & editing, Writing – original draft, Visualization, Validation, Software, Resources, Methodology, Investigation, Formal analysis, Data curation, Conceptualization. **Jari Böling:** Writing – review & editing, Writing – original draft, Methodology, Funding acquisition. **Roberto Vettor:** Writing – review & editing, Writing – original draft, Methodology, Data curation.

Ethical approval

This paper is the author's original work and has not been previously published elsewhere.

Declaration of Generative AI and AI-assisted technologies in the writing process

During the preparation of this work, the authors used ChatGPT and Microsoft Copilot to refine the language and improve clarity. After using this tool, the authors reviewed and edited the content as needed and take full responsibility for the content of the publication.

Funding

This research was supported by Business Finland through the project *INDECS – Integration of Design and Operation of Cruise Ship Energy Systems* (Grant No. 7682/31/2022).

Declaration of competing interest

The authors declare that they have no conflicts of interest regarding the publication of this research article. The research was conducted in the absence of any commercial or financial relationships that could be construed as a potential conflict of interest.

Acknowledgments

The authors express their appreciation to the reviewers for their thorough assessment and helpful feedback, which undoubtedly enhanced the paper's quality.

Data availability

The authors do not have permission to share data.

References

[1] W. Ma, J. Zhang, Y. Han, T. Mao, D. Ma, B. Zhou, M. Chen, A decision-making optimization model for ship energy system integrating emission reduction regulations and scheduling strategies, J. Ind. Inf. Integr. 35 (2023) 100506, http://dx.doi.org/10.1016/j.jii.2023.100506, URL https://www.sciencedirect.com/science/article/pii/S2452414X23000791.

[2] R. Vettor, C.G. Soares, Reflecting the uncertainties of ensemble weather forecasts on the predictions of ship fuel consumption, Ocean Eng. 250 (2022) 111009, http://dx.doi.org/10.1016/j.oceaneng.2022.111009.

[3] M. Bilušić, L. Olivari, Assessment of process chain suitability of the optical 3D measuring system by using influencing factors for measurement uncertainty, J. Ind. Inf. Integr. 41 (2024) 100654, http://dx.doi.org/10.1016/j.jii.2024.100654, URL https://www.sciencedirect.com/science/article/pii/S2452414X24000980.

[4] K. Mahmoodi, H. Ghassemi, H. Nowruzi, M.M. Shora, Prediction of the hydrodynamic performance and cavitation volume of the marine propeller using gene expression programming, Ships Offshore Struct. 14 (7) (2019) 723–736, http://dx.doi.org/10.1080/17445302.2018.1557589.

[5] K. Mahmoodi, J. Böling, A. Razminia, R. Vettor, Investigating the effects of weather condition uncertainties on the required propulsion power of a cruise ship, Ships Offshore Struct. (2025) 1–21, http://dx.doi.org/10.1080/17445302.2025.2545909, arXiv:https://doi.org/10.1080/17445302.2025.2545909.

[6] K. Mahmoodi, J. Böling, R. Vettor, Evaluating the influence of marine weather parameters uncertainties on the ship fuel consumption with Monte Carlo analysis, Ocean Eng. 341 (2025) 122531, http://dx.doi.org/10.1016/j.oceaneng.2025.122531, URL https://www.sciencedirect.com/science/article/pii/S0029801825022140.

[7] K. Mahmoodi, A. Razminia, H. Ghassemi, Optimal control of wave energy converters with non-integer order performance indices: A dynamic programming approach, Renew. Energy 177 (2021) 1212–1233, http://dx.doi.org/10.1016/j.renene.2021.06.045, URL https://www.sciencedirect.com/science/article/pii/S0960148121009113.

[8] N.S. Abbasian, A. Salajegheh, H. Gaspar, P.O. Brett, Improving early OSV design robustness by applying 'Multivariate Big Data Analytics' on a ship's life cycle, J. Ind. Inf. Integr. 10 (2018) 29–38, http://dx.doi.org/10.1016/j.jii.2018.02.002, URL https://www.sciencedirect.com/science/article/pii/S2452414X17300869.

[9] S. Mirjalili, S.M. Mirjalili, A. Lewis, Grey wolf optimizer, Adv. Eng. Softw. 69 (2014) 46–61, http://dx.doi.org/10.1016/j.advengsoft.2013.12.007, URL https://www.sciencedirect.com/science/article/pii/S0965997813001853.

[10] S. Mirjalili, S. Saremi, S.M. Mirjalili, L. dos S. Coelho, Multi-objective grey wolf optimizer: A novel algorithm for multi-criterion optimization, Expert Syst. Appl. 47 (2016) 106–119, http://dx.doi.org/10.1016/j.eswa.2015.10.039, URL https://www.sciencedirect.com/science/article/pii/S0957417415007435.

[11] M.S. Shaikh, C. Wang, S. Xie, G. Zheng, X. Dong, S. Qiu, M.A. Ahmad, S. Raj, Coverage and connectivity maximization for wireless sensor networks using improved chaotic grey wolf optimization, Sci. Rep. 15 (1) (2025) 15706, http://dx.doi.org/10.1038/s41598-025-00184-2.

[12] I. Dagal, A.-W. Ibrahim, A. Harrison, W.F. Mbasso, A.O. Hourani, I. Zaitsev, Hierarchical multi step Gray Wolf optimization algorithm for energy systems optimization, Sci. Rep. 15 (1) (2025) 8973, http://dx.doi.org/10.1038/s41598-025-92983-w.

[13] J. Lu, R. Feng, X. Pan, M. Zhang, W. Ma, J. Gao, Self-recovery regulation method of rotor unbalance vibration based on GWO-ALQR, Chin. J. Mech. Eng. 39 (2026) 100021, http://dx.doi.org/10.1016/j.cjme.2025.100021, URL https://www.sciencedirect.com/science/article/pii/S1000934525000215.

[14] M.A. Ahmad, G. Yoganathan, M.I. Mohd Rashid, M.R. Hao, M.H. Suid, M.Z. Mohd Tumari, Improved smoothed functional algorithms- optimized PID controller for efficient speed regulation of wind turbines, IEEE Trans. Ind. Appl. 61 (5) (2025) 7546–7560, http://dx.doi.org/10.1109/TIA.2025.3550137.

[15] S. Saat, M.A. Ahmad, M.R. Ghazali, Data-driven brain emotional learning-based intelligent controller-PID control of MIMO systems based on a modified safe experimentation dynamics algorithm, Int. J. Cogn. Comput. Eng. 6 (2025) 74–99, http://dx.doi.org/10.1016/j.ijcce.2024.11.005, URL https://www.sciencedirect.com/science/article/pii/S2666307424000494.

[16] N.M.Z.A. Mustapha, M.A. Ahmad, Normalized SPSA for Hammerstein model identification of twin rotor and electro-mechanical positioning systems, Int. J. Cogn. Comput. Eng. 6 (2025) 552–568, http://dx.doi.org/10.1016/j.ijcce.2025.04.004, URL https://www.sciencedirect.com/science/article/pii/S2666307425000233.

[17] J. Wang, X. Zhang, W. Guo, Z. Yang, N. Anselem Tengecha, Disruption management-based coordinated scheduling for vessels and ship loaders in bulk ports, Adv. Eng. Informatics 56 (2023) 101989, http://dx.doi.org/10.1016/j.aei.2023.101989, URL https://www.sciencedirect.com/science/article/pii/S1474034623001179.

[18] X. Zhang, R. Li, C. Wang, B. Xue, W. Guo, Robust optimization for a class of ship traffic scheduling problem with uncertain arrival and departure times, Eng. Appl. Artif. Intell. 133 (2024) 108257, http://dx.doi.org/10.1016/j.engappai.2024.108257, URL https://www.sciencedirect.com/science/article/pii/S0952197624004159.

[19] Z. Elmi, B. Li, B. Liang, Y. yip Lau, M. Borowska-Stefańska, S. Wiśniewski, M.A. Dulebenets, An epsilon-constraint-based exact multi-objective optimization approach for the ship schedule recovery problem in liner shipping, Comput. Ind. Eng. 183 (2023) 109472, http://dx.doi.org/10.1016/j.cie.2023.109472, URL https://www.sciencedirect.com/science/article/pii/S0360835223004965.

[20] S. Li, T. Wang, How emissions trading system affects liner ship disruption recovery, Transp. Policy 169 (2025) 191–208, http://dx.doi.org/10.1016/j.tranpol.2025.05.004, URL https://www.sciencedirect.com/science/article/pii/S0967070X25001830.

[21] Z. Elmi, B. Li, A.M. Fathollahi-Fard, G. Tian, M. Borowska-Stefańska, S. Wiśniewski, M.A. Dulebenets, Ship schedule recovery with voluntary speed reduction zones and emission control areas, Transp. Res. D 125 (2023) 103957, http://dx.doi.org/10.1016/j.trd.2023.103957, URL https://www.sciencedirect.com/science/article/pii/S1361920923003541.

[22] M. Asghari, M.Y. Jaber, S. Mirzapour Al-e-hashem, Coordinating vessel recovery actions: Analysis of disruption management in a liner shipping service, European J. Oper. Res. 307 (2) (2023) 627–644, http://dx.doi.org/10.1016/j.ejor.2022.08.039, URL https://www.sciencedirect.com/science/article/pii/S0377221722006828.

[23] J. Zheng, C. Mao, Y. Li, Y. Liu, Y. Wang, Dynamic vessel schedule recovery strategy of liner shipping with uncertainties: An event-triggered model predictive control solution, Comput. Ind. Eng. 193 (2024) 110340, http://dx.doi.org/10.1016/j.cie.2024.110340, URL https://www.sciencedirect.com/science/article/pii/S0360835224004613.

[24] J. Wang, X. Zhao, R. Huang, A two-stage learning-based approach incorporating sustainable port multi-resource scheduling and real-time disruption response under mixed loading mode, Adv. Eng. Informatics 67 (2025) 103513, http://dx.doi.org/10.1016/j.aei.2025.103513, URL https://www.sciencedirect.com/science/article/pii/S1474034625004069.

[25] T.P. Zis, H.N. Psaraftis, L. Ding, Ship weather routing: A taxonomy and survey, Ocean Eng. 213 (2020) 107697, http://dx.doi.org/10.1016/j.oceaneng.2020.107697, URL https://www.sciencedirect.com/science/article/pii/S0029801820306879.

[26] C. Gkerekos, I. Lazakis, A novel, data-driven heuristic framework for vessel weather routing, Ocean Eng. 197 (2020) 106887, http://dx.doi.org/10.1016/j.oceaneng.2019.106887, URL https://www.sciencedirect.com/science/article/pii/S0029801819309722.

[27] D. Ma, W. Ma, S. Jin, X. Ma, Method for simultaneously optimizing ship route and speed with emission control areas, Ocean Eng. 202 (2020) 107170, http://dx.doi.org/10.1016/j.oceaneng.2020.107170, URL https://www.sciencedirect.com/science/article/pii/S0029801820302298.

[28] A. De, J. Wang, M.K. Tiwari, Hybridizing basic variable neighborhood search with particle swarm optimization for solving sustainable ship routing and bunker management problem, IEEE Trans. Intell. Transp. Syst. 21 (3) (2020) 986–997, http://dx.doi.org/10.1109/TITS.2019.2900490.

[29] K. Kurosawa, Y. Uchiyama, T. Kosako, Development of a numerical marine weather routing system for coastal and marginal seas using regional oceanic and atmospheric simulations, Ocean Eng. 195 (2020) 106706, http://dx.doi.org/10.1016/j.oceaneng.2019.106706, URL https://www.sciencedirect.com/science/article/pii/S0029801819308200.

[30] K. Hein, Y. Xu, G. Wilson, A.K. Gupta, Coordinated optimal voyage planning and energy management of all-electric ship with hybrid energy storage system, IEEE Trans. Power Syst. 36 (2021) 2355–2365, http://dx.doi.org/10.1109/TPWRS.2020.3029331, URL https://api.semanticscholar.org/CorpusID:233333354.

[31] M. Grifoll, C. Borén, M. Castells-Sanabra, A comprehensive ship weather routing system using CMEMS products and A* algorithm, Ocean Eng. 255 (2022) 111427, http://dx.doi.org/10.1016/j.oceaneng.2022.111427, URL https://www.sciencedirect.com/science/article/pii/S0029801822008095.

[32] W. Du, Y. Li, G. Zhang, C. Wang, B. Zhu, J. Qiao, Ship weather routing optimization based on improved fractional order particle swarm optimization, Ocean Eng. 248 (2022) 110680, http://dx.doi.org/10.1016/j.oceaneng.2022.110680, URL https://www.sciencedirect.com/science/article/pii/S0029801822001408.

[33] D. Ma, S. Zhou, Y. Han, W. Ma, H. Huang, Multi-objective ship weather routing method based on the improved NSGA-III algorithm, J. Ind. Inf. Integr. 38 (2024) 100570, http://dx.doi.org/10.1016/j.jii.2024.100570, URL https://www.sciencedirect.com/science/article/pii/S2452414X24000141.

[34] X. Chen, R. Hu, K. Luo, H. Wu, S.A. Biancardo, Y. Zheng, J. Xian, Intelligent ship route planning via an A* search model enhanced double-deep Q-network, Ocean Eng. 327 (2025) 120956, http://dx.doi.org/10.1016/j.oceaneng.2025.120956, URL https://www.sciencedirect.com/science/article/pii/S0029801825006699.

[35] E.M. Bitner-Gregersen, S.K. Bhattacharya, I.K. Chatjigeorgiou, I. Eames, K. Ellermann, K. Ewans, G. Hermanski, M.C. Johnson, N. Ma, C. Maisondieu, A. Nilva, I. Rychlik, T. Waseda, Recent developments of ocean environmental description with focus on uncertainties, Ocean Eng. 86 (2014) 26–46, http://dx.doi.org/10.1016/j.oceaneng.2014.03.002, Uncertainty Modelling for Ships and Offshore Structures. URL https://www.sciencedirect.com/science/article/pii/S002980181400081X.

[36] L. Aldous, T. Smith, R. Bucknall, P. Thompson, Uncertainty analysis in ship performance monitoring, Ocean Eng. 110 (2015) 29–38, http://dx.doi.org/10.1016/j.oceaneng.2015.05.043, Energy Efficient Ship Design and Operations. URL https://www.sciencedirect.com/science/article/pii/S0029801815002437.

[37] T. Plessas, A. Papanikolaou, S. Liu, N. Adamopoulos, The effect of weather uncertainties on ship's fuel consumption, in: SNAME International Symposium on Ship Operations, Management and Economics, SNAME, 2018, pp. SNAME–SOME.

[38] J.T. Hunsucker, D. Przelomski, A. Bashkoff, J. Dixon, L. Shipwright, Uncertainty analysis of methods used to measure ship fuel oil consumption, Int. Marit. Organ. MEPC 72 (2018) URL https://wwwcdn.imo.org/localresources/en/OurWork/Environment/Documents/Uncertainty_Analysis_in_Ship_Fuel_Oil_Consumption.pdf.

[39] F. Tillig, J.W. Ringsberg, W. Mao, B. Ramne, Analysis of uncertainties in the prediction of ships' fuel consumption–from early design to operation conditions, Ships Offshore Struct. 13 (sup1) (2018) 13–24, http://dx.doi.org/10.1080/17445302.2018.1425519.

[40] T.A. Tran, Effects of the uncertain factors impacting on the fuel oil consumption of sea ocean-going vessels based on the hybrid multi criteria decision making method, Ocean Eng. 239 (2021) 109885, http://dx.doi.org/10.1016/j.oceaneng.2021.109885, URL https://www.sciencedirect.com/science/article/pii/S0029801821012336.

[41] T. Dickson, H. Farr, D. Sear, J.I.R. Blake, Uncertainty in marine weather routing, Appl. Ocean Res. 88 (2019) 138–146, http://dx.doi.org/10.1016/j.apor.2019.04.008, URL https://www.sciencedirect.com/science/article/pii/S0141118719300380.

[42] H. Wang, X. Lang, W. Mao, D. Zhang, G. Storhaug, Effectiveness of 2D optimization algorithms considering voluntary speed reduction under uncertain metocean conditions, Ocean Eng. 200 (2020) 107063, http://dx.doi.org/10.1016/j.oceaneng.2020.107063, URL https://www.sciencedirect.com/science/article/pii/S0029801820301360.

[43] R. Vettor, G. Bergamini, C. Guedes Soares, A comprehensive approach to account for weather uncertainties in ship route optimization, J. Mar. Sci. Eng. 9 (12) (2021) http://dx.doi.org/10.3390/jmse9121434, URL https://www.mdpi.com/2077-1312/9/12/1434.

[44] M. Li, C. Xie, X. Li, A. Karoonsoontawong, Y.-E. Ge, Robust liner ship routing and scheduling schemes under uncertain weather and ocean conditions, Transp. Res. C 137 (2022) 103593, http://dx.doi.org/10.1016/j.trc.2022.103593, URL https://www.sciencedirect.com/science/article/pii/S0968090X22000390.

[45] R. Szlapczynski, J. Szlapczynska, R. Vettor, Ship weather routing featuring w-MOEA/D and uncertainty handling, Appl. Soft Comput. 138 (2023) 110142, http://dx.doi.org/10.1016/j.asoc.2023.110142, URL https://www.sciencedirect.com/science/article/pii/S1568494623001606.

[46] J. Ksciuk, S. Kuhlemann, K. Tierney, A. Koberstein, Uncertainty in maritime ship routing and scheduling: A literature review, European J. Oper. Res. 308 (2) (2023) 499–524, http://dx.doi.org/10.1016/j.ejor.2022.08.006, URL https://www.sciencedirect.com/science/article/pii/S037722172200649X.

[47] Ü. Öztürk, M. Akdağ, T. Ayabakan, A review of path planning algorithms in maritime autonomous surface ships: Navigation safety perspective, Ocean Eng. 251 (2022) 111010, http://dx.doi.org/10.1016/j.oceaneng.2022.111010, URL https://www.sciencedirect.com/science/article/pii/S0029801822004334.

[48] N. Charalambopoulos, E. Xidias, A. Nearchou, Efficient ship weather routing using probabilistic roadmaps, Ocean Eng. 273 (2023) 114031, http://dx.doi.org/10.1016/j.oceaneng.2023.114031, URL https://www.sciencedirect.com/science/article/pii/S0029801823004158.

[49] Q. Liu, Y. Wang, R. Zhang, H. Yan, J. Xu, Y. Guo, Arctic weather routing: a review of ship performance models and ice routing algorithms, Front. Mar. Sci. 10 (2023) http://dx.doi.org/10.3389/fmars.2023.1190164, URL https://www.frontiersin.org/journals/marine-science/articles/10.3389/fmars.2023.1190164.

[50] CruiseMapper, CruiseMapper - cruise ship tracker, 2024, URL https://www.cruisemapper.com/. (Accessed 03 October 2024).

[51] G.C. Group, GEBCO 2024 grid, 2024, Global terrain model for ocean and land, providing elevation data at a 15 arc-second interval grid. URL https://www.gebco.net/data_and_products/gridded_bathymetry_data/.

[52] Open-Meteo, Open-Meteo: Free Weather API, 2024, https://open-meteo.com. (Accessed 20 September 2024).

[53] Deutscher Wetterdienst, Deutscher Wetterdienst (DWD), 2024, https://www.dwd.de. (Accessed 20 September 2024).

[54] A.D. Bull, Convergence rates of efficient global optimization algorithms, 2011, arXiv:1101.3501. URL https://arxiv.org/abs/1101.3501.

[55] J. Snoek, H. Larochelle, R.P. Adams, Practical Bayesian optimization of machine learning algorithms, 2012, arXiv:1206.2944. URL https://arxiv.org/abs/1206.2944.

[56] M.A. Gelbart, J. Snoek, R.P. Adams, Bayesian optimization with unknown constraints, 2014, arXiv:1403.5607. URL https://arxiv.org/abs/1403.5607.

[57] K. Mahmoodi, E. Nepomuceno, A. Razminia, Wave excitation force forecasting using neural networks, Energy 247 (2022) 123322, http://dx.doi.org/10.1016/j.energy.2022.123322, URL https://www.sciencedirect.com/science/article/pii/S0360544222002250.

[58] K. Mahmoodi, H. Nowruzi, Extreme wave height detection based on the meteorological data, using hybrid NOF-ELM method, Ships Offshore Struct. 17 (11) (2022) 2520–2530, http://dx.doi.org/10.1080/17445302.2018.1557589.

[59] G. Vittori, Y. Falkouskaya, D.M. Jimenez-Gutierrez, T. Cattai, I. Chatzigiannakis, Graph neural networks to model and optimize the operation of water distribution networks: A review, J. Ind. Inf. Integr. 47 (2025) 100880, http://dx.doi.org/10.1016/j.jii.2025.100880, URL https://www.sciencedirect.com/science/article/pii/S2452414X25001037.

[60] J. Nocedal, S.J. Wright, Numerical Optimization, second ed., in: Numerical Mathematics and Scientific Computation, vol. 2, Springer, New York, NY, 2006, p. XXII, 664, http://dx.doi.org/10.1007/978-0-387-40065-5.

[61] B. Mohseni-Gharyehsafa, S. Hussain, A. Fahy, M. De Rosa, F. Pallonetto, A hybrid Gaussian process-integrated deep learning model for retrofitted building energy optimization in smart city ecosystems, Appl. Energy 388 (2025) 125643, http://dx.doi.org/10.1016/j.apenergy.2025.125643, URL https://www.sciencedirect.com/science/article/pii/S0306261925003733.

[62] MathWorks - MATLAB and simulink for technical computing, 2024, https://www.mathworks.com/. (Accessed 30 December).

[63] S. Kaur, Y. Kumar, A. Koul, S. Kumar Kamboj, A systematic review on metaheuristic optimization techniques for feature selections in disease diagnosis: open issues and challenges, Arch. Comput. Methods Eng. 30 (3) (2022) 1863–1895, http://dx.doi.org/10.1007/s11831-022-09853-1.

[64] M.H. Nadimi-Shahraki, H. Zamani, Z. Asghari Varzaneh, A.S. Sadiq, S. Mirjalili, A systematic review of applying grey wolf optimizer, its variants, and its developments in different internet of things applications, Internet Things 26 (2024) 101135, http://dx.doi.org/10.1016/j.iot.2024.101135, URL https://www.sciencedirect.com/science/article/pii/S2542660524000775.

[65] S.N. Makhadmeh, M.A. Al-Betar, I.A. Doush, M.A. Awadallah, S. Kassaymeh, S. Mirjalili, R.A. Zitar, Recent advances in grey wolf optimizer, its versions and applications: Review, IEEE Access 12 (2024) 22991–23028, http://dx.doi.org/10.1109/ACCESS.2023.3304889.

[66] A. Akter, E.I. Zafir, N.H. Dana, R. Joysoyal, S.K. Sarker, L. Li, S.M. Muyeen, S.K. Das, I. Kamwa, A review on microgrid optimization with meta-heuristic techniques: Scopes, trends and recommendation, Energy Strat. Rev. 51 (2024) 101298, http://dx.doi.org/10.1016/j.esr.2024.101298, URL https://www.sciencedirect.com/science/article/pii/S2211467X24000051.

[67] H. Faris, I. Aljarah, M.A. Al-Betar, S. Mirjalili, Grey wolf optimizer: a review of recent variants and applications, Neural Comput. Appl. 30 (2018) 413–435, http://dx.doi.org/10.1007/s00521-017-3272-5.

[68] A. Agarwal, A. Chandra, S. Shalivahan, R.K. Singh, Grey wolf optimizer: a new strategy to invert geophysical data sets, Geophys. Prospect. 66 (6) (2018) 1215–1226, http://dx.doi.org/10.1016/j.eswa.2015.10.039.

[69] I.M.S. Committee, Revised guidance to the master for avoiding dangerous situations in adverse weather and sea conditions, 2007, IMO Circular MSC.1/Circ. 1228, Approved at the eighty-second session (29 November - 8 December 2006).

[70] PIANC, Harbour Approach Channels Design Guidelines, MarCom Report Report No. 121, The World Association for Waterborne Transport Infrastructure, Brussels, Belgium, 2014.